Online Estimation of Key Parameters for Settling Slurries

by

Dana Rose Moon

A thesis submitted in partial fulfillment of the requirements for the degree of

Master of Science
in
Process Control

Department of Chemical and Materials Engineering
University of Alberta

Abstract

Heterogeneous slurry pipelines are found in mining, chemical, and solid transportation (such as coal pipelines) industries worldwide. One of the most important factors in the operation and design of these pipelines is bulk velocity. Solids settle when the bulk velocity is below the deposition velocity. This can cause plugging, equipment damage, and production downtime. Since the actual particle size distribution is typically unknown online, pipelines are usually operated at excessively high velocities to mitigate the risk of settling. This causes erosion and additional energy use.

Specific energy consumption (SEC) is a measure of the energy required to transport one tonne of solids a distance of one kilometer. It is highly dependent on solids properties, such as average solids size and coarse solids concentration. Presently, there is no way to predict all solids properties online accurately.

Solids properties and pipeline parameters are often used as inputs into steady-state slurry models to predict the pressure gradient and other slurry flow properties. The most commonly used is the two-layer model developed by the Saskatchewan Research Council (SRC). In this model, the slurry is approximated as two step functions that horizontally split the pipe into two layers. The pressure gradient is calculated by considering Coulombic and kinematic friction.

In this study, an interior-point optimization algorithm is used to estimate coarse solids median particle size and concentration using the Saskatchewan Research Council two-layer model for turbulent, heterogeneous, and Newtonian slurries. The parameters were estimated using the SRC

two-layer model to simulate a sand/water slurry in a 75.65 mm diameter pipe. A narrow particle size distribution was used with coarse solids concentration volume fractions of 0.1 to 0.4. The coarse solids median particle size was varied between 75 to 625 μm in 25 μm intervals. The values were chosen to most accurately reflect slurries found in the mining and oil sands industries. For the purposes of optimization studies, the decision variables were also the parameters to be estimated. The estimated coarse solids median particle size and concentration were compared with inputs used in the Saskatchewan Research Council two-layer model.

The average error for coarse solids median particle size and concentration predictions were 13.6% and 4.2%, respectively. The error from the predicted values propagated through deposition velocity calculations. The predictions for the deposition velocity had 5.5% average error. The SEC prediction trends matched the known SEC trends, and the minimum SEC could be predicted graphically with close agreement to the known minimum.

Future work includes experimental validation. It is necessary to use process instruments including a flowmeter, a differential pressure transducer, and a densitometer to provide inputs for the estimation method. A velocity profiler can be used to estimate the top and bottom velocities; however, further studies are required to determine the best way to determine the velocity variables from the sensors. Additionally, a system of elliptic PDEs may be able to predict velocity variables instead of using a velocity profiler. Furthermore, the same estimation method can also be applied to a new SRC model that has particle size distributions (rather than a median value only) as an input.

To my parents.

Work hard and be kind.

Acknowledgements

Thank you to my two supervisors Dr. Fraser Forbes and Dr. Sean Sanders. Meetings with Fraser always fostered critical thinking and were consistently the best part of my day. The technical knowledge and professional skills he taught me will be applied throughout my career and personal life. Sean always challenged and supported me. If it was not for him, I would not have had the opportunities or confidence to be successful.

My thesis benefited from the unique opportunity to work with the Saskatchewan Research Council (SRC), and especially from Dr. Ryan Spelay's guidance and help. It was an honor to work with them.

I gratefully acknowledge the Natural Science and Engineering Research Council of Canada (NSERC) Industrial Chair for Pipeline Transport Processes for financially supporting this project.

I am very grateful to Dr. Arno de Klerk, Terry Runyon, Roohi Shorki, and Rebecca Latimer for their various forms of help, support, and advice.

Thank you to Tahseen Mushtaque for being the definition of a best friend. The laughter and support is much appreciated and acknowledged in getting me through life.

The University of Alberta community - the programs, groups, activities, and people - had a monumental impact on my personal growth; thank you.

Table of Contents

List of Tables

List of Figures

1 Introduction

1.1 Slurry Pipelines

Slurries are found worldwide in the mining and mineral processing industries (Derammelaere, 2014; Harris and Talamudpula, 2014). Examples include dredging, precious metal mining, and oil sands mines. In the United States there are approximately 8 000 km of slurry pipelines that have been constructed primarily for iron, copper, and coal slurries (Derammelaere, 2014). In 2004, half a million tonnes of solids flowed per day in the Alberta oil sands (Sanders et al., 2004). Since that time, existing operations have expanded (e.g. Shell's Jackpine Mine) and new mines have begun production (e.g. Imperial Oil's Kearl Lake). In these mines, slurries are transported long distances from mines to processing plants and waste mixtures are pipelined to disposal sites.

Slurries consist of solid particles in a liquid carrier fluid and are, generally, categorized as non-settling or settling (Paterson and Cooke, 2014; Gillies, 1993). Non-settling slurries are usually composed of particles with diameters less than 74 μm (Shook et al., 2002) and typically exhibit non-Newtonian behavior at high solids concentrations. The pressure gradient and flow characteristics can often be predicted with modified single-phase models (Gillies, 1993).

Slurries found in the oil sands industry often consist of particle diameters between 180-300 μm (Schaan et al., 2007). They are considered settling slurries. For these types of slurries, the coarse solids will deposit when suspension forces are too low (i.e. when operating velocities are too

low). This can result in pipeline plugging, equipment damage, and production outages (Albion et al., 2011). Additionally, the pressure gradient and flow characteristics are highly dependent on particle diameter, particle shape, solids concentration, and bulk velocity, and cannot be predicted accurately with modified single-phase models (Shook et al., 2002). A pressure gradient prediction model used worldwide in the oil sands and pipeline design industry is the Saskatchewan Research Council (SRC) two-layer model (Sanders et al., 2004). This model treats the system at steady-state, and the slurry properties are used as constant inputs.

1.2 Problem Statement

The SRC two-layer model requires information about the slurry solid properties. A designed (or expected) slurry is used as a basis in calculations; however, in operations, the solids properties vary from the designed case, which will change the pressure gradient and deposition velocity calculations. The true dynamic system can be represented by continuously updating the calculations. Presently, this is not possible, because instantaneous and accurate measurements of all the required slurry properties are typically not available. Therefore, slurry pipelines are often operated at excessively high velocities, primarily to prevent deposition of solid particles; however, this accelerates pipeline wear and wastes energy.

Velocity can be lowered toward, but not below, the deposition velocity (the velocity at which solids begin to settle). Lowering the velocity will reduce pipeline wear and energy use. Deposition velocity will not always correspond to the most efficient velocity to operate a pipeline (Hashemi, 2014b). Specific Energy Consumption (SEC) is a quantity describing the efficiency of transporting solids in a slurry pipeline, and is defined as the energy required to

transport one tonne of solids one kilometer. The lower the SEC is the more efficient pipeline operation becomes (Wilson et al., 2005).

1.3 Thesis Objectives

The main objective of this research is to estimate the coarse solids median diameter, $d_{50,}$ and concentration, C_r, online. The d_{50} and C_r values are used as inputs in the SRC two-layer model; however, back-calculating their values are analytically impossible due to the complicated forms of the equations in the model.

Optimization techniques are often used when equations become too complicated to be solved analytically. Optimization was initially documented as early as ancient Rome (Edgar et al., 2001), but it did not become widely used until World War II to solve logistics problems (Forbes and Aksikas, 2010a). Optimization is now heavily relied upon in the oil and gas industry and has many applications, such as improving plant performance, reducing maintenance costs, and maximizing profit (Edgar et al., 2001). For example, optimization techniques saved more than 30 million dollars annually when applied to gasoline blending in a Texaco refinery in the 1980s (Adhya et al., 1999).

In this study, an interior-point optimization algorithm is applied to coarse particle (settling) slurry pipelines. The specific objectives of this project are as follows:

1. To develop an estimation method to predict d_{50} and C_r.
2. To determine how the predicted d_{50} and C_r affect deposition velocity and SEC predictions.

1.4 Thesis Outline

The thesis is organized in the manner described below. Slurry properties, pressure gradient, and SEC are described in Chapter 2. The process model is described in Chapter 3. The optimization technique and simulation results are detailed in Chapter 4. Instrumentation that can be used for future implementation of the estimation method is discussed in Chapter 5. In Chapter 6, conclusions and recommendations are made.

2 Slurry Properties and Specific Energy Consumption

In this chapter, slurry properties are defined and relationships among slurry properties, pressure gradient, and SEC are formed. The relationships are chiefly based upon pipeline pressure gradient being a function of many slurry properties, including d_{50}, C_r, and bulk velocity.

Slurry pipeline pressure gradients are strongly related to the size of the solid particles in the mixture. Particles found in industrial slurries are rarely monosized, and therefore particle size distributions (PSD) are used to describe the size range of solid particles. Usually, PSDs are a graph that plots the fraction of particles in the slurry on the vertical axis and the size of particles on the horizontal axis. A cumulative frequency PSD has a vertical axis corresponds to the fraction of particles in the slurry that have diameters smaller than the value on the horizontal axis. Therefore, the particle with the largest diameter will have a cumulative frequency of 1, because all other particles are smaller (Crowe, 2006). The particle size that corresponds to the median size has a cumulative frequency of 0.5. A particle size that corresponds to the median size of only the coarse particles (discuss further in this section) is called the d_{50}. Furthermore, a PSD also describes how much particle sizes vary in a slurry. A monodispersed PSD is considered to have solids of approximately the same size (Crowe, 2006). Monodispersed PSDs have a geometric standard deviation of 1. A narrow PSD usually has a geometric standard deviation less than 1.5 (Kaushal and Tomita, 2013). PSDs with larger standard geometric deviations are considered broad. Figure 1 provides data from Paterson and Cooke (2014) for three different PSDs for tailings, kimberlite, and sand slurry samples. The tailings and kimberlite are considered to have broad PSDs. The sand sample is considered to have a narrow PSD, and has a mass

median particle size of the entire solids (coarse and fines) of approximately 200 µm. It should be noted that the PSDs in Figure 1 are for illustration purposes only, since each of these three mineral slurries can have broad PSDs with a variety of d_{50} sizes.

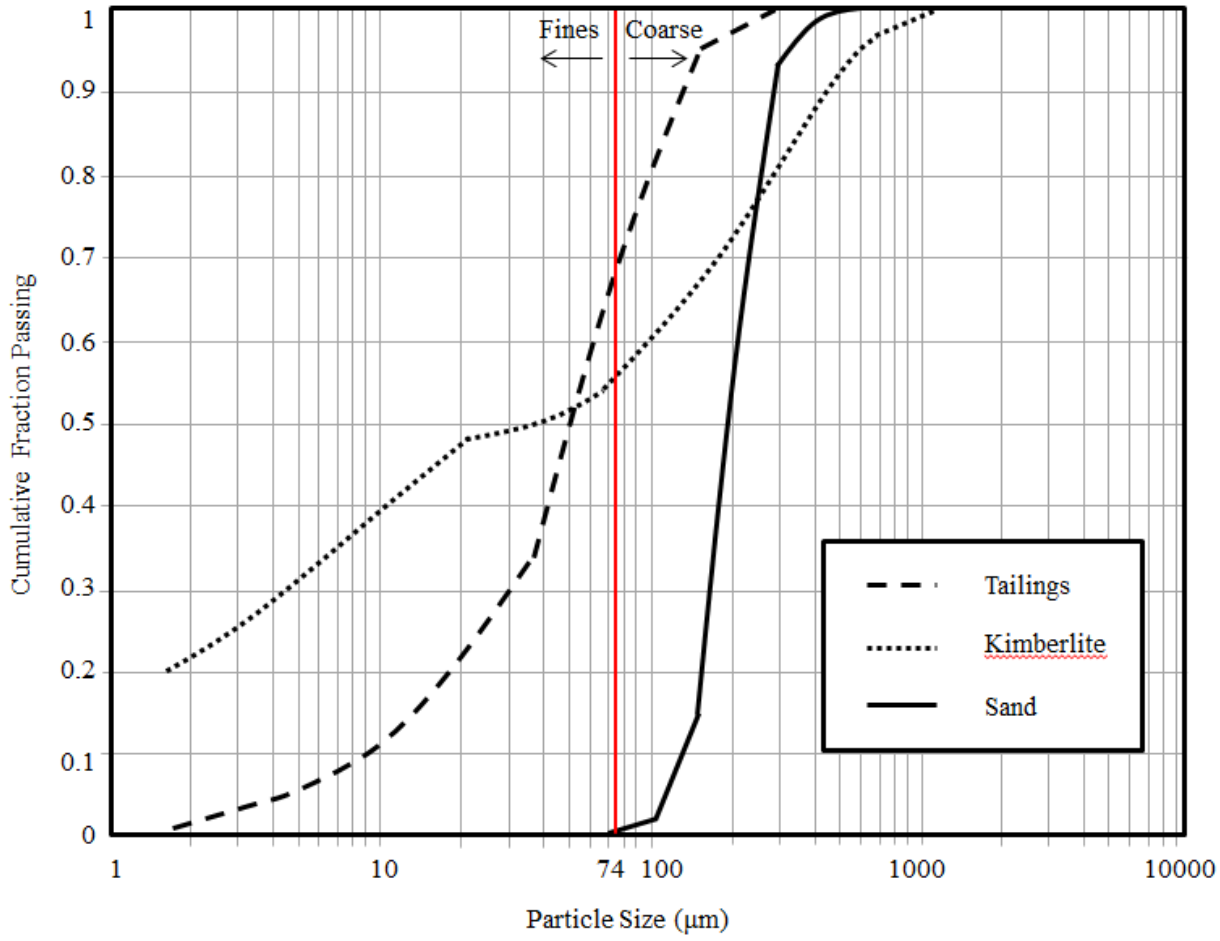

Figure 1: Particle size distributions (Paterson and Cooke, 2014; Rhodes, 2008)

The PSD can be split into two general particle sizes; coarse and fines, illustrated in Figure 1. The fine particles are defined to be particles with a diameter less than 74 µm and are "assumed to be distributed uniformly within the pipe" (Shook et al., 2002). The designation between fine and

coarse particles becomes an important factor when calculating the pressure gradient, especially in regards to the concentration of particles. The volumetric solids concentration is defined by:

$$C_t = \frac{\text{volume of solids}}{\text{volume of solids} + \text{volume of liquid}} \tag{2.1}$$

The total solid concentration includes fine, C_{rf}, and coarse, C_r, particles:

$$C_t = C_{rf} + C_r \tag{2.2}$$

The solids particle size, solids concentration, and bulk velocity highly influence the pressure gradient and the slurry behavior (Crowe, 2006; Matousek, 2004; Matousek, 1997; Brown, 1991; Durand and Condolios, 1952). These properties affect whether turbulent eddies will fully suspend or partially suspend solid particles. Particles that are not completely suspended are supported by the pipe wall (Vlasak et al., 2014). The solids concentration at the pipe invert will be higher than at the top of the pipe, creating an asymmetrical vertical velocity profile (Vlasak et al., 2014). This is referred to as partially-stratified flow or heterogeneous flow (Wilson et al., 2005). As the vertical velocity and concentration profiles become more asymmetric, the flow becomes more stratified, which is illustrated in Figure 2.

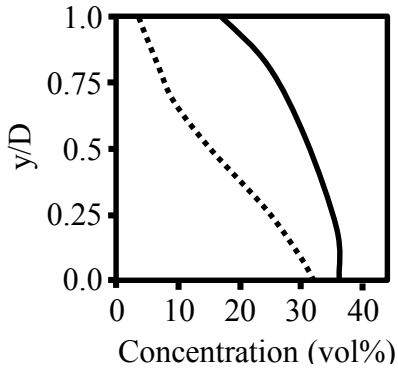

Figure 2: Vertical concentration profile of sand slurries that are stratified (solid line) and highly stratified (dashed line). Data from Gillies and Shook (1994): d_{50} = 190 μm sand; V = 3.7 m/s; C_t = 0.16 (dashed line) and C_t = 0.30 (solid line).

As previously mentioned, heterogeneous flow is characterized by an asymmetrical vertical velocity profile (Hashemi, 2013). This means that solid particles are moving at different vertical speeds and are not uniformly distributed vertically. Therefore, the solids concentration inside of the pipeline will differ from the solids concentration at the outlet of the pipeline (Wilson et al., 2005). The delivered solids concentration, C_{vd}, is the solids concentration discharged at the outlet of the pipe (Shook et al., 2002):

$$C_{vd} = \frac{1}{AV}\int_{A} cv_s dA \tag{2.3}$$

where v_s is the local time averaged vertical particle velocity, and c is the local solids volume fraction (Saskatchewan Research Council, 2014). The in-situ concentration represents the mean solids volumetric concentration at any pipe cross-section (Saskatchewan Research Council,

2014). In the SRC two-layer model, the in-situ concentration is the same as the coarse solids concentration, which will be discussed in Section (3.2).

$$C_r = \frac{1}{A}\int_A c dA \tag{2.4}$$

The asymmetry of the vertical velocity and concentration profiles are functions of the bulk velocity, which is perhaps the most critical parameter in the design and operation of a pipeline (Matousek, 1997) due to its strong relation with the pressure gradient and solids deposition (Crowe, 2006; Matousek, 2004; Matousek, 1997; Brown, 1991; Durand and Condolios, 1952). The bulk velocity, V, is defined as:

$$V = \frac{4Q}{\pi D^2} \tag{2.5}$$

where Q is the total volumetric flowrate in the pipe, and D is the inside diameter of the pipe. Particles settle if the bulk velocity is less than V_c. This increases friction, because the stationary deposit reduces the cross sectional area available for flow. This means that the pressure gradient will increase when the bulk velocity is lower than the deposition velocity (Shook and Roco, 1991). Alternatively, when the velocity is sufficiently increased past V_c, there is enough turbulent forces to prevent deposition (King, 2002). The pressure gradient will continue to increase as the bulk velocity increases.

The shape of the pressure gradient versus bulk velocity curve will differ in relation to V_c depending on the slurry properties. The minimum pressure gradient will correspond to V_c for

settling slurries that have a d_{50} less than approximately 100 μm (Hashemi et al., 2010). For coarser particles, V_c is less than the velocity which the minimum pressure gradient occurs. This is because a shear layer exists for highly stratified slurries that forms between the particle-dense and particle-lean areas of the pipe (Matousek, 1997). The shear layer becomes thicker when the velocity is slightly above V_c. In this layer there is interparticle contact that assists in suspending the particles in combination with turbulence. This reduces the pressure gradient further as the velocity is increased above V_c (Matousek, 1997).

Pressure gradient versus bulk velocity curves are drawn in Figure 3 for slurries containing different particle sizes. The vertical lines on Figure 3 illustrate the V_c for each slurry, and the slurries with median particle diameters of 400 and 600 μm have approximately the same V_c. Slurries with median particle sizes of 90 and 150 μm have a minimum pressure gradient that corresponds to V_c, but coarser particles have a minimum pressure gradient at a velocity higher than V_c (Hashemi, 2014b; Hashemi, 2010; Matousek, 1997).

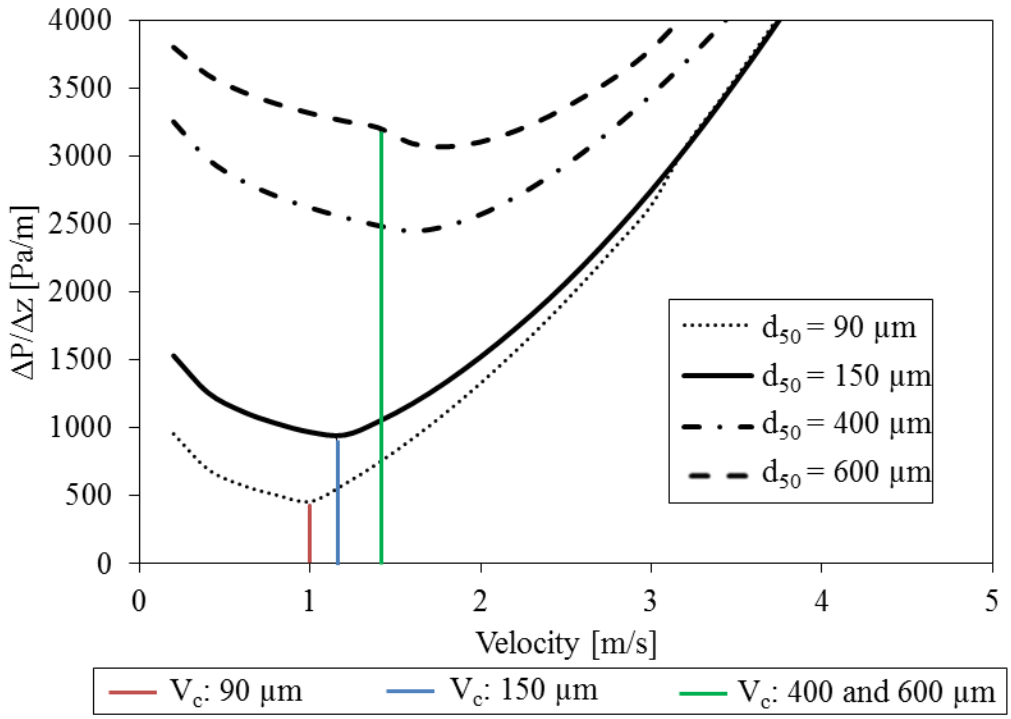

Figure 3: Pressure gradients and deposition velocities for sand-in-water slurries with particle sizes of 90, 150, 400, and 600 µm, with C_{vd} =0.30, C_f =0.03, ρ_s = 2650 kg/m^3, and D = 0.05 m

Pumps increase the pressure within the pipeline, and are needed to overcome friction losses and/or elevation increases. Generally speaking, pumps can be used to control the bulk velocity at which the slurry moves through the pipe (De Nevers, 2005). The power [W] that a pump provides to the slurry can be written as:

$$\text{Power} = H_m Q \rho_m g \tag{2.6}$$

where H_m is the head of the mixture, and ρ_m is the density of the solid-liquid mixture. The head of the mixture can be written as:

$$H_m = -\frac{\Delta P}{\Delta z}\frac{1}{\rho_m g}L \tag{2.7}$$

In slurry pipelines, the solids are the payload to be transported; whereas, the liquid is the medium to transport the solids (Wilson et al., 2005). The power requirement in Equation (2.6) is in terms of the solid-liquid mixture. Therefore, a different parameter should be used to describe the efficiency of transporting the solids. Specific Energy Consumption (SEC) [J/kg/m] is defined as the energy required to transport one tonne of solids over one kilometer (Wilson et al., 2005):

$$SEC = \frac{Power}{\rho_s C_{vd} Q L} \tag{2.8}$$

Since the most important design parameters are bulk velocity, solids concentration, and particle diameter, system SEC is often shown as a function of these parameters. This can be achieved by substituting Equations (2.7) and (2.6) into Equation (2.8):

$$SEC = \frac{\Delta P}{\Delta z}\frac{1}{C_{vd}\rho_s} \tag{2.9}$$

Therefore, SEC is a function of the pressure gradient, delivered solids concentration, and solids density.

Figure 4 is a plot of predicted SEC for sand-water slurries having d_{50} values of 90, 150, 400, and 600 μm. The vertical line indicates the predicted V_c, and the V_c for 400 and 600 μm are approximately the same. The values were obtained by using the SRC two-layer model (described in Chapter 3) with values for C_{vd} = 0.30, C_f = 0.03, ρ_s = 2650 kg/m^3, k = 0.045 mm, and D = 0.05

m. The minimum SEC increases as d_{50} increases. This is because as d_{50} increases, the particles supported by the pipe wall increases (Matousek, 1997).

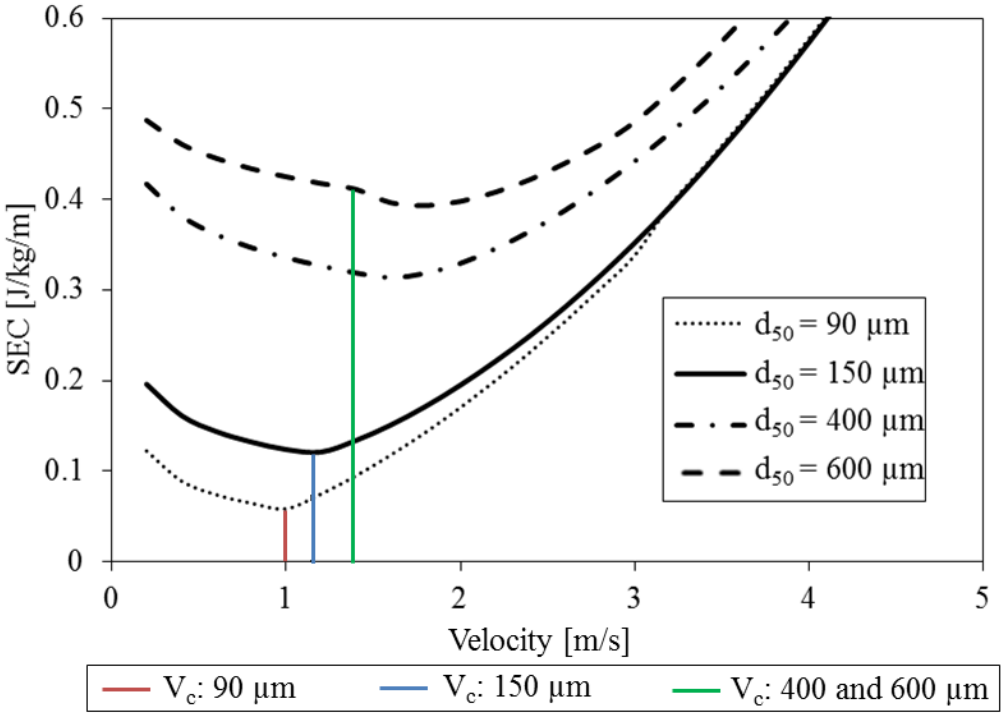

Figure 4: SEC versus velocity for d_{50} values of 90, 150, 400, and 600 µm with C_{vd} = 0.30, C_f = 0.03, ρ_s = 2650 kg/m^3, k = 0.045 mm, D = 0.05 m, and water as the carrier fluid

Figure 5 is a plot of predicted SEC for sand-water slurries with the delivered coarse solids concentration (C_{vd}) set at values of 0.12, 0.30, and 0.40. The vertical line indicates the predicted V_c. The values were obtained for d_{50} = 90 µm, D = 0.05m, C_f = 0.01, and ρ_s = 2650 kg/m^3 using the SRC two-layer model. It has been found that the minimum SEC occurs when the volumetric solids concentration is approximately 30% (Hashemi et al., 2010). This indicates that it is more energy efficient to not over dilute or over concentrate the slurry.

Figure 6 is a plot of predicted SEC values for a sand-water slurry flowing in pipelines 0.05, 0.0635, and 0.0762 m in diameter. The vertical line indicates the predicted V_c. The values were obtained by using the SRC two-layer model for d_{50} = 90 µm, C_{vd} = 0.30, C_f = 0.03, k = 0.045 mm, ρ_s = 2650 kg/m^3, and a carrier liquid of water. The minimum SEC decreases as diameter increases. This is an important design consideration. Usually slurry pipelines are designed such that a certain solids production rate is reached. Therefore, with the velocity and solids properties known, the pipeline can be designed with a diameter that results in the minimum SEC.

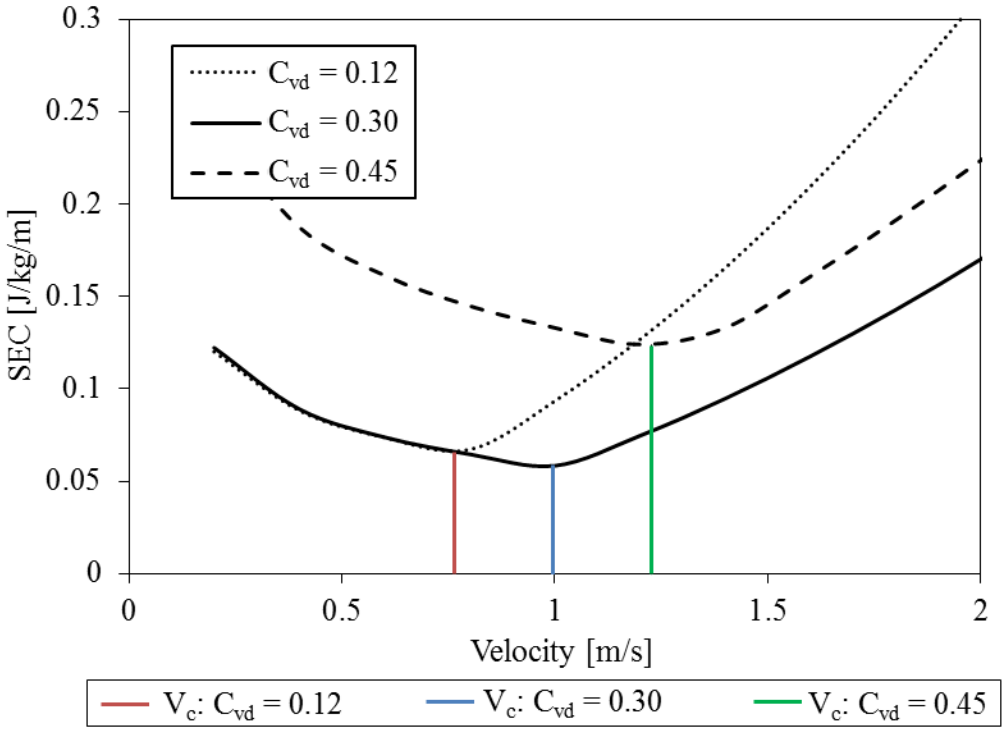

Figure 5: SEC versus velocity for total solids volumetric concentrations of 0.12, 0.30, and 0.40 with d_{50} = 90 µm, C_f = 0.01, ρ_s = 2650 kg/m^3, k = 0.045 mm, D = 0.05 m, and water as the carrier fluid

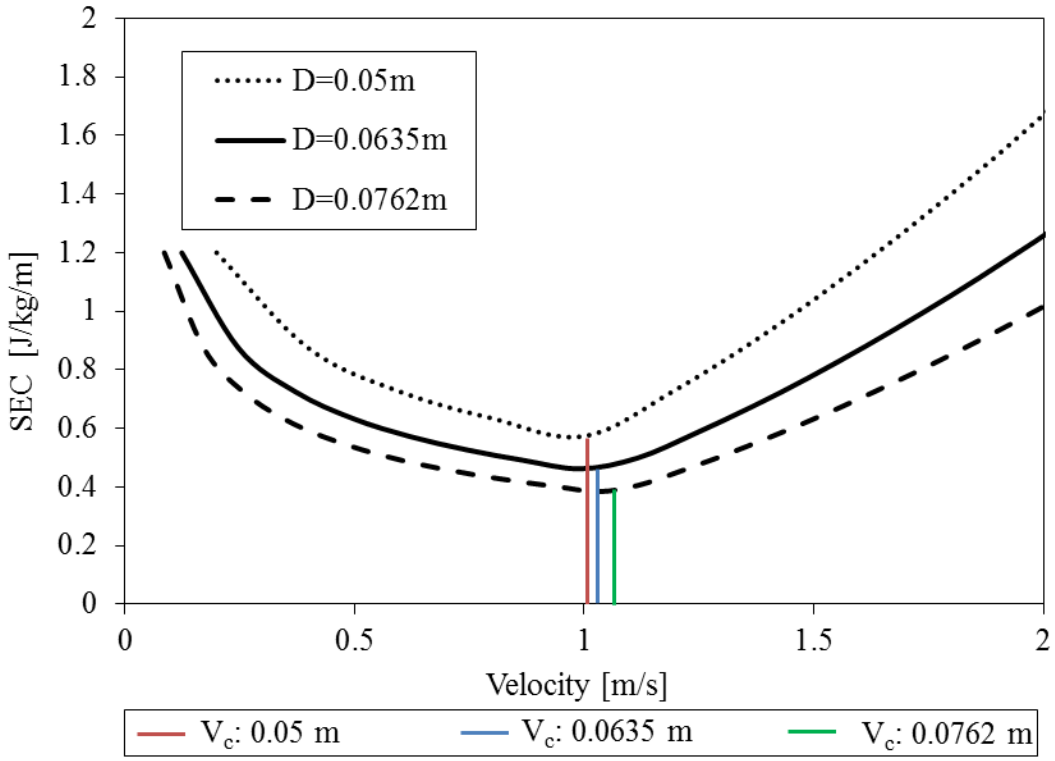

Figure 6: SEC versus velocity for pipeline diameters of 0.05, 0.0635, and 0.0762 m with d_{50} = 90 µm, C_{vd} = 0.30, C_f = 0.03, k = 0.045 mm, and ρ_s = 2650 kg/m^3, with water as the carrier fluid

The pressure gradient in slurry pipelines is highly influenced by the bulk velocity, solids concentration, and particle size. One of the most important slurry pipeline parameters is the bulk velocity, as it affects the pressure gradient and stratification ratio. The efficiency of the pipeline system can be measured using the SEC, which can be calculated from the pressure gradient, delivered solids concentration, and solids density (as previously described). By predicting the median coarse solids diameter and coarse solids concentration, it would be possible to calculate SEC instantaneously to optimize the pipeline operation.

3 Modelling

In this chapter, two-layer models are investigated for the purpose of d_{50} and C_r estimation. In two-layer models, the slurry pipeline is modelled by a top and bottom section. The estimation method uses the semi-mechanistic steady-state SRC two-layer model to predict d_{50} and C_r. Therefore, it is necessary to understand this model thoroughly. A system of partial differential equations that use a two-layer assumption is also derived to capture transient behavior and to calculate layer properties.

3.1. Two-Layer Models

Slurries can be modelled with first principle approaches using continuity and momentum equations for the liquid and solid phases. These equations have been extensively used in the field of CFD simulations (Messa et al., 2014), and can model transient three-dimensional slurry behavior (Kalekudithi et al., 2009). As of yet, the models are not able to detect the minimum pressure gradient or model behavior for all slurry types, and are complex in that additional coupling terms, averaging techniques, or treatment of the two phases as separate continuum are required to solve them (Messa et al., 2014; Kalekudithi et al., 2009; Krampa, 2009). Presently, the CFD solve times are often thirty minutes of CPU time or more (Messa et al., 2014). For these reasons, first principle approaches are not employed for online applications and cannot at this time be used directly for SEC minimization.

A layered approximation can be used to overcome the issues of complexity and reduce solutions times in modelling slurries. The layered approximation originated in 1970, when Wilson (1970a) performed force-balances on a model developed by Newitt et al. (1955) that predicted slurry pressure drop based on fluid friction and friction caused by particles on the pipe wall. Wilson (1976) approximated the flow behavior by splitting the pipe into two horizontal sections. This approach resulted in various versions of layered models (Gillies et al., 1991), but generally the bottom layer contains particles that contribute to friction at the pipe wall (contact load). All fine particles (particles with a diameter less than 74 μm) are "assumed to be distributed uniformly within the pipe" (Shook et al., 2002). The fine particles change the fluid properties and are not included in the vertical concentration profile. Furthermore, the vertical concentration and velocity profiles are approximated by step functions. The top layer is represented with a uniform concentration, C_1, which moves at mean velocity, V_1. The same approximation is made for the bottom layer, with C_2 and V_2. The areas of the top and bottom layers are represented by A_1 and A_2, respectively. A schematic representation of the model is shown in Figure 7.

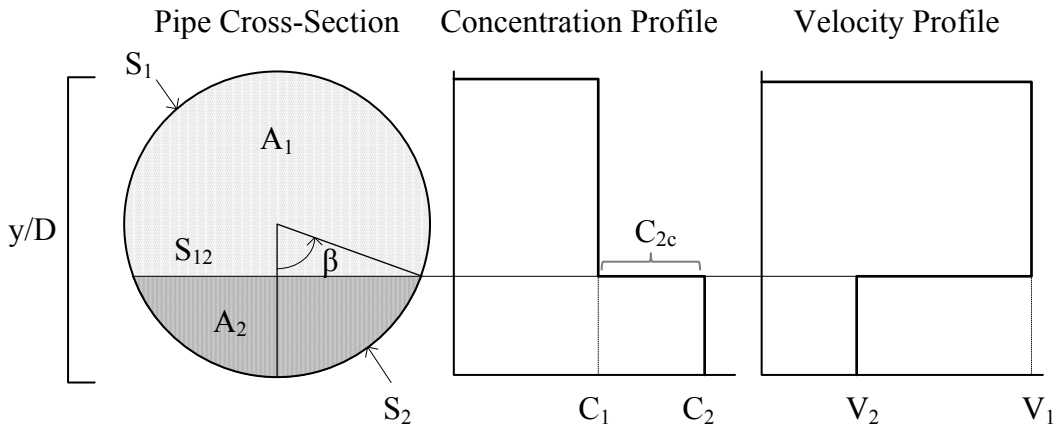

Figure 7: Two-layer model schematic

The friction associated with the pressure gradient is often split into velocity independent and velocity dependent factors (Shook et al., 2002). Coulombic friction is caused by particles that are not completely suspended by turbulence that are contacting the pipe wall (Matousek, 1996; Shook and Roco, 1991), and are referred to as contact load. Kinematic friction is also considered, which describes velocity-dependent friction, and includes particle dispersive stress and near-wall lift (Sanders, 2012). Dispersive stresses force particles towards the wall, and are related to particle collisions as the solids concentration increases (Hashemi, 2013). Friction is reduced by near-wall lift that forces particles away from the wall, and increases as d_{50} and bulk velocity increase (Hashemi et al., 2014b). This is summarized in Figure 8.

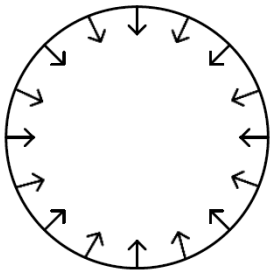

Near-Wall Lift

- Particles forces away from the wall
- Decreases kinematic friction
- Increases with velocity
- Increases with particle size
- Not significant if particles are smaller than the viscous sublayer

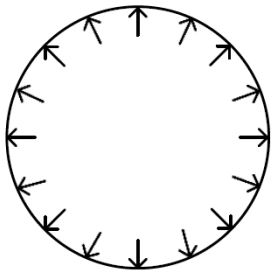

Particle Dispersive Stress

- Forces particles toward the wall
- Related to particle interations
- Increases kinematic friction
- Increases with solids concentration

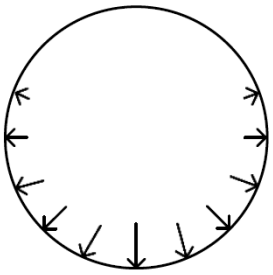

Coulombic Friction

- Solids are supported by pipe wall
- Occurs when turbulence cannot suspend all particles
- Calculated from the normal stress of particles in contact with each other, i.e. the immersed weight of the coarse particles not supported by fluid turbulence

Figure 8: Components of friction in slurry flow (Hashemi et al., 2014b; Hashemi 2013; Sanders, 2012; Shook and Roco, 1991)

3.2. Steady-State Model

3.2.1. Pressure Gradient

The Saskatchewan Research Council (SRC) two-layer model is used to predict the pressure gradient and deposition velocity for heterogeneous slurry flow in horizontal pipes. The SRC two-layer model is one of many layered models originating from a force-balance model from Wilson (1970a). This model will be used in this study because it is commonly utilized for slurry pipeline design and industrial operations worldwide (Sanders et al., 2004), and predicts the pressure gradient well for a wide variety of settling slurries (Spelay et al., 2013). The SRC two-layer model describes slurry properties semi-mechanistically (Kalekudithi et al., 2009; Sanders et al., 2004). Certain parameters that vary with pipe diameter (Shook et al., 2002) are derived empirically. The empirical correlations were determined from SRC experiments performed for C_{vd} up to 0.46 and d_{50} from 85 μm to 2400 μm (Gillies et al., 2004; Gillies and Shook, 2000; Gillies et al., 1991). The SRC two-layer model is continuously improved upon as new experiments are performed and new physical models are proposed (Sanders, 2012). The version used in this study is PipeFlow 10.

The SRC two-layer model was first presented by Gillies et al. (1991), and adapts the model from Wilson (1976) for slurries with Coulombic friction. PipeFlow 10 also includes near-wall lift and particle dispersive stresses (Shook et al., 2002). The model requires the inputs of Q, d_{50}, C_r, C_{max}, k, D, ρ_s, ρ_f, and μ_f. The PipeFlow 10 model takes d_{50} to be the median particle diameter of the coarse solids fraction (occasionally referred to as d_{50c}), and assumes that all of the coarse particles have the same size (Sanders et al., 2004). The SRC two-layer model is summarized graphically in Figure 9, and is described in greater detail in this section.

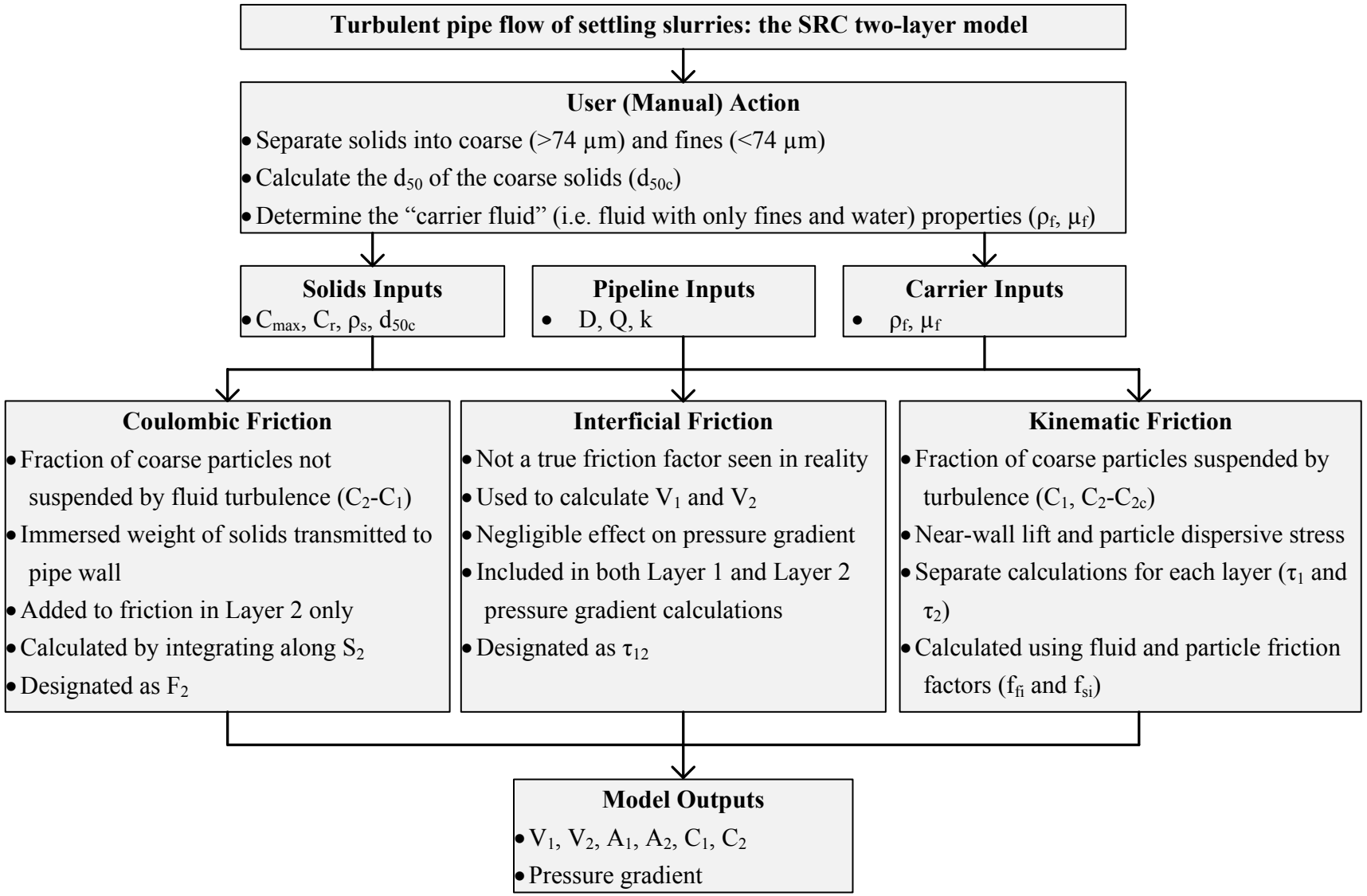

Figure 9: Summary of the SRC two-layer model (Hashemi, 2013; Paterson and Cooke, 2014; Shook et al., 2002)

The SRC two-layer model considers partially stratified flow as opposed to fully stratified flow. Fully stratified flow has no particles in the upper layer, and the lower layer only has particles in contact with each other (Matousek, 1996). Partially stratified flow occurs when the upper layer contains particles suspended by turbulence, at concentration C_1, and the lower layer contains particles suspended by turbulence and contact load, at concentration C_2.

In the SRC two-layer model, the areas, concentrations, and velocities are predicted based upon the stratification ratio. It is defined by the contact load concentration, C_c, divided by the in-situ coarse solids concentration, C_r. This stratification ratio is determined by (Gillies et al., 2004; Saskatchewan Research Council, 2014):

$$\frac{C_c}{C_r} = \exp\left(-0.076\left(\frac{V}{V_\infty}\right)^{0.77}\left(\frac{V}{\sqrt{gD(\rho_s/\rho_m - 1)}}\right)^{-0.36}\right) \tag{3.1}$$

where V_∞ is the terminal settling velocity of a single particle in the fluid, and is calculated using a specific correlation for sand grains (Shook et al., 2002). Since C_1 contains only particles supported by turbulence, the stratification ratio can be used to solve for C_1 (Gillies et al., 2004):

$$C_1 = C_r\left(1 - \frac{C_C}{C_r}\right) \tag{3.2}$$

Not only is C_1 the coarse solids concentration in Layer 1, but it also represents the particles supported by turbulence in Layer 2. The coarse solids concentration of Layer 2, C_2, can be calculated using the concentration profile and semi-empirical algorithms, as presented in Gillies

and Shook (1994), and taken to be the value at y/D=0.15. The concentration of contact load in the lower layer, C_{2c} (Matousek, 1996), is found by subtracting C_1 from C_2.

In the SRC two-layer model, the carrier fluid properties must be manually calculated. The carrier fluid density should be taken as:

$$\rho_f = C_f\rho_s + (1 - C_f)\rho_L \tag{3.3}$$

where C_f is the solids volumetric concentration of fines in the liquid as though there were no coarse particles (Gillies and Shook, 2000; Gillies, 1993; Gillies et al., 1991). It is defined as:

$$C_f = \frac{C_{rf}}{(1 - C_t) + C_{rf}} \tag{3.4}$$

Figure 10 summarizes all of the concentrations discussed in the SRC two-layer model.

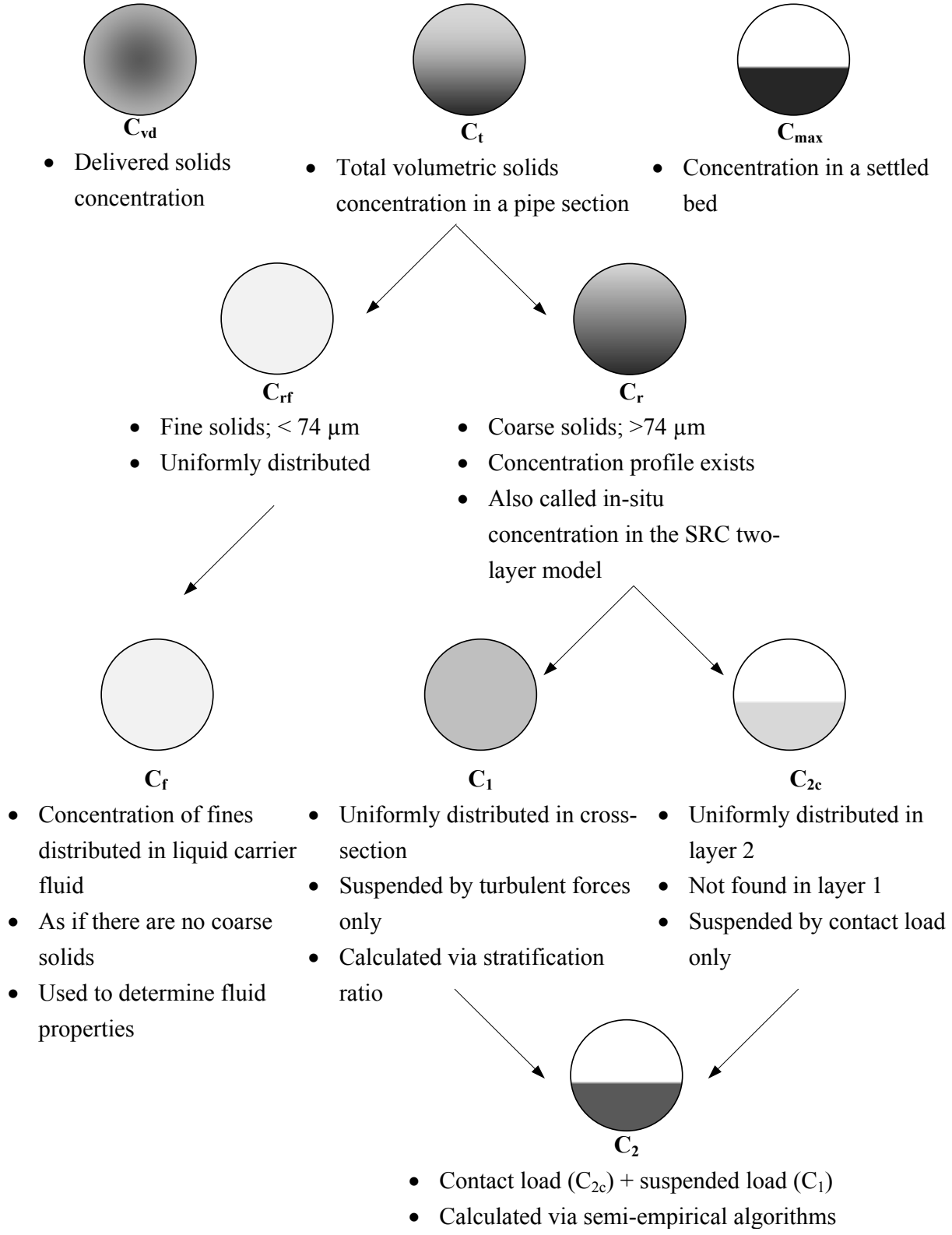

Figure 10: Summary of concentrations found in the SRC two-layer model (Matousek, 1997; Gillies 1993)

The remainder of the model consists of mass and momentum balance equations for both layers. The set of mass and momentum balances is solved via iteration. The pressure gradients in the upper and lower layers must be equal, and are calculated by force balances over the shear stresses that act on the layers' perimeters (Shook et al., 2002):

$$-\frac{dP}{dz} = \frac{\tau_1 S_1 + \tau_{12} S_{12}}{A_1} \tag{3.5}$$

$$-\frac{dP}{dz} = \frac{\tau_2 S_2 - \tau_{12} S_{12} + F_2}{A_2} \tag{3.6}$$

where S_1, S_2, and S_{12} are the partial parameters, and F_2 is the Coulombic friction. The Coulombic friction is calculated via the shear stress from particle-wall contact, τ_C, which is related to the normal stress at the pipe wall, σ (Sanders, 2012 and Matousek, 1997):

$$\tau_C = \eta_s \sigma \tag{3.7}$$

where η_s is the coefficient of friction between the particles and pipe wall. The normal stress varies with vertical position (Wilson et al., 2005; Matousek, 1997; Wilson et al., 1972; Wilson, 1970b):

$$\frac{d\sigma}{dy} = \eta_s g C_{2c} (\rho_s - \rho_f) \tag{3.8}$$

This normal stress acts in the radial direction in horizontal pipelines. Therefore, integrating over the height of the bed using cylindrical coordinates with $y=0.5D(1-\cos\alpha)$, where α is the angle

normal to the pipe wall, gives the normal stress at the pipe wall (Matousek, 1997). The total force exerted on the pipe wall by Layer 2 is calculated by integrating along the pipeline perimeter (S_2) using β:

$$F_2 = D\eta_s \int_0^{\beta} \sigma d\alpha = 0.5gD^2\eta_s(\rho_s - \rho_1)C_{2c}(\sin(\beta) - \beta\cos(\beta)) \tag{3.9}$$

This procedure is illustrated in Figure 11:

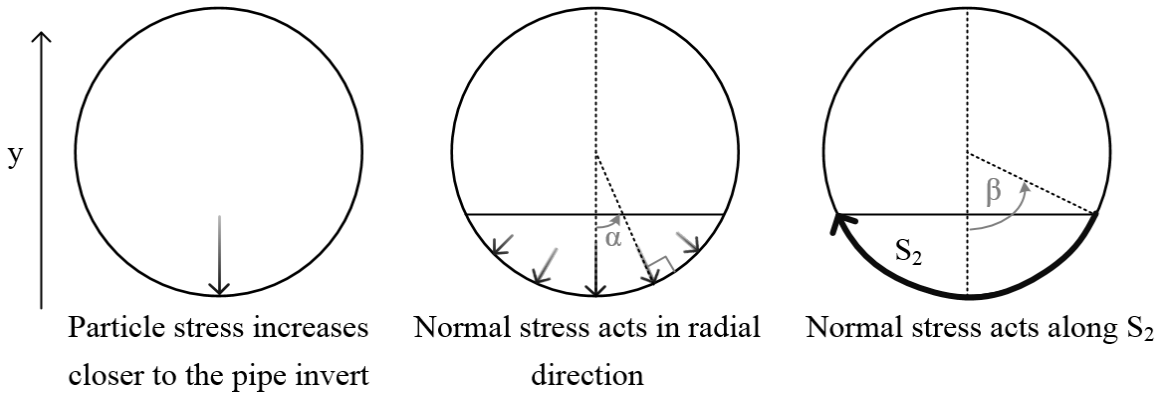

Figure 11: Steps to calculate Coulombic friction (Sanders, 2012; Matousek, 1997)

Note that η_s depends on the slurry and wall properties. Shook et al. (1982) determined the value to be 0.5 for sand slurries that is adjusted using the following expression (Saskatchewan Research Council, 2014):

$$\eta_s = 0.5\left(1 + 0.005\lambda_{Cr}^{2.5}\right) \tag{3.10}$$

where λ is the linear concentration of solids, and represents the ratio of the particle diameter over the average distance between neighboring particles (Shook et al., 2002):

$$\lambda_i = \left[\left(\frac{C_{max}}{C_i}\right)^{1/3} - 1\right]^{-1} \tag{3.11}$$

where C_{max} is the solids volume fraction in a settled bed, and the subscript i represents Layer 1 or Layer 2. The density of Layer 1, ρ_1, is calculated by:

$$\rho_1 = C_1\rho_s + (1 - C_1)\rho_f \tag{3.12}$$

The kinematic, or velocity dependent stresses are symbolized by τ_1 and τ_2. They oppose motion and act at the pipe wall in their respective layers. The following equation incorporates dispersive stresses and lift effects (Gillies, 2013):

$$\tau_i = 0.5V_i^2(f_{si}\rho_s + f_{fi}\rho_f) \tag{3.13}$$

where f_{fi} is the fluid friction factor, and can be calculated via the Churchill equation for Fanning friction factor using the fluid density and viscosity. The particle friction factor, f_{si}, is calculated using the correlation from Gillies (2013):

$$f_{si} = \begin{cases} \lambda_i^{1.25}[-0.00011\ln(d_i^+) + 0.00042] & d_i^+ \leq 21 \\ \lambda_i^{1.25}[-0.000056\ln(d_i^+) + 0.00026] & 21 < d_i^+ \leq 100 \\ 0 & d_i^+ > 100 \end{cases} \tag{3.14}$$

where d^+ is the dimensionless particle diameter:

$$d^+_i = d_{50} V_i \left(\frac{f_{fi}}{2}\right)^{0.5} \frac{\rho_f}{\mu_f} \tag{3.15}$$

As previously stated, the vertical concentration and velocity profiles in two-layer models are approximated by step functions. This creates an interface between Layer 1 and Layer 2. An interface is not present in reality. While the interfacial stress, τ_{12}, is included in the pressure gradient equations, it has negligible effect on the pressure gradient; it is included for the calculation of the velocities in the two layers (Shook et al., 2002). The interface is treated as a surface with roughness proportional to the particle diameter at the interface, d_{12} (Matousek, 1997):

$$\tau_{12} = 0.5 f_{12} (V_1 - V_2)^2 \rho_1 \tag{3.16}$$

The interfacial friction factor, f_{12}, is based on Nikuradse's friction equation for rough boundaries (Matousek, 1997) and was modified based on experimental data by Gillies et al. (1991) to yield:

$$f_{12} = \frac{2(1 + k1)}{\left[3.36 + 4 \log_{10}\left(\frac{d_{12}}{D}\right)\right]^2} \tag{3.17}$$

$$k1 = \begin{cases} 0 & \frac{d_{12}}{D} < 0.002 \\ 5 + 1.86 \log_{10}\left(\frac{d_{12}}{D}\right) & \text{otherwise} \end{cases} \tag{3.18}$$

The mass and material balances that the model must also satisfy are (Shook et al., 2002):

$$AV = A_1V_1 + A_2V_2 \tag{3.19}$$

$$C_{vd}AV = C_1A_1V_1 + C_2A_2V_2 \tag{3.20}$$

$$C_rV = C_1V_1 + C_2V_2 \tag{3.21}$$

3.2.2. Deposition Velocity Predictions

The SRC two-layer model also includes equations to predict V_c. The same equations will be used to calculate V_c in this study, as the equations developed by the SRC are for conditions found in the mining and mineral processing industries (Spelay et al., 2014). The accuracy of these predictions is expected to be within 0.3 m/s (Saskatchewan Research Council, 2014). There are three equations used by the SRC two-layer model. They are for coarse, intermediate, and fine particles, which are defined by the Archimedes number (Gillies et al., 2000):

$$Ar = \frac{4gd_{50}^3\rho_f(\rho_s - \rho_f)}{3\mu_f^2} \tag{3.22}$$

The form of most correlations use the Froude number, F, which was originally proposed by Durand and Condolios (1952). The Froude number definition used in the SRC model is (Saskatchewan Research Council, 2014):

$$V_c = F\sqrt{gD\frac{\rho_s - \rho_f}{\rho_f}} \tag{3.23}$$

If Ar ≥ 125 then the particles are considered coarse (i.e., typically when the d_{50} is between 90 and 4000 μm (Paterson and Cooke, 2014)). The deposition velocity is controlled mainly by inertial forces and the following correlation is used (Paterson & Cooke, 2014; Saskatchewan Research Council, 2014):

$$\begin{array}{cc} F = 1.35 & Ar \geq 86000 \\ F = 2.35 - 0.088\ln Ar & 2690 \leq Ar < 86000 \\ F = 1.27 + 0.049\ln Ar & 125 \leq Ar < 2690 \end{array} \tag{3.24}$$

If Ar < 125 and $d^+ > 5$, then the particles are considered to be intermediate. The deposition velocity in this region depends on inertial and viscous forces. Interpolation is used between the viscous and inertial force calculations (Saskatchewan Research Council, 2014). If Ar < 125 and $d^+ \leq 5$, then the particles are considered to be "fine", and the deposition velocity is a function of the viscous sublayer (Saskatchewan Research Council, 2014). Since most slurries in the oil sands industry have a d_{50} between 180 to 300 μm (Schaan et al., 2007) and fall in the inertial category, intermediate and fine particles will not be discussed in any detail here. Further information can be found in Shook et al. (2002), Paterson and Cooke (2014), the SRC's course notes for the two-layer model (Saskatchewan Research Council, 2014), and Thomas (2014).

In this study, the estimation method used to predict d_{50} and C_r uses equations in the SRC two-layer model. The model has been derived to predict the pressure gradient, which includes kinematic and Coulombic friction, given that slurry properties (including d_{50} and C_r) are

provided. The slurry properties of d_{50} and C_r are also required for deposition velocity predictions. The deposition velocity equation that will be used in this study was also developed by the SRC for slurries in the mining and mineral processing industries (Spelay et al., 2014). Since the SRC two-layer model is a steady-state model, it does not include information about transient conditions and does not consider different slurries mixing in the pipeline. Transient conditions are addressed in the next section, and the consequences of not considering mixing are discussed in Chapter 5.

3.3. Transient Model

Slurry pipeline flow has been described with many different solid-liquid models. Models that are often used in the mining and oil sands industries are steady-state models, such as the SRC two-layer model (Sanders et al., 2004). These are steady-state rather than dynamic (transient) models. In reality, slurry properties change as a function of time and space, which means that slurry pipelines can be classified as a distributed parameter system (DPS). Partial differential equations (PDEs) include time and space derivatives and can be used to describe DPS dynamics.

Speranza (2001) performed mass and momentum balances over a two-layer model, and used a three-layer model for simulations with explicit Euler methods. The models developed from Speranza (2001) will not be directly used in this study, because they were derived with the assumption that density is constant in each layer. This assumption results in constant concentration in the second layer, which directly impacts Coulombic friction and the pressure gradient. Sinkov et al. (2014) also modelled slurry pipeline dynamics using a layered approximation for heterogeneous flow and flow with a stationary bed.

Using the two-layer assumption, as presented in Figure 7, mass and momentum balances were performed. The solid mass balances for Layer 1 and Layer 2 are:

$$\frac{\partial C_1 A_1 \rho_s D}{\partial t} + \frac{\partial C_1 A_1 V_1 \rho_s D}{\partial z} = -m_{s12} + m_{s21} \tag{3.25}$$

$$\frac{\partial C_2 A_2 \rho_s D}{\partial t} + \frac{\partial C_2 A_2 V_2 \rho_s D}{\partial z} = m_{s12} - m_{s21} \tag{3.26}$$

where m_{s12} is the mass transfer of solid from Layer 1 into Layer 2 due to gravitational forces, and m_{s21} is the mass transfer of solid from Layer 2 into Layer 1 due to particles being suspended by turbulence. A momentum balance for the solid-liquid mixture was also performed:

$$\frac{\partial V_1 A_1 \rho_1}{\partial t} + V_1 \frac{\partial V_1 A_1 \rho_1}{\partial z} = A_1 \left[-\frac{dP}{dz}\right] - \tau_1 S_1 - \tau_{12} S_{12} - M_{12} + M_{21} \tag{3.27}$$

$$\frac{\partial V_2 A_2 \rho_2}{\partial t} + V_2 \frac{\partial V_2 A_2 \rho_2}{\partial z} = A_2 \left[-\frac{dP}{dz}\right] - \tau_2 S_2 + \tau_{12} S_{12} - F_2 + M_{12} - M_{21} \tag{3.28}$$

where M_{12} is the momentum transfer from Layer 1 to 2, and M_{21} is the momentum transfer from Layer 2 to 1. Equations (3.25) and (3.26) were added together, and Equations (3.27) and (3.28) were combined along with Equations (3.5) and (3.6) to yield:

$$\frac{\partial (C_1 A_1 + C_2 A_2)}{\partial t} + \frac{\partial (C_1 A_1 V_1 + C_2 A_2 V_2)}{\partial z} = 0 \tag{3.29}$$

$$\frac{\partial(\rho_1 A_1 V_1 + \rho_2 A_2 V_2)}{\partial t} + V_1 \frac{\partial V_1 A_1 \rho_1}{\partial z} + V_2 \frac{\partial V_2 A_2 \rho_2}{\partial z} = 0 \tag{3.30}$$

Equations (3.29) and (3.30) have eight variables (A_1, A_2, C_1, C_2, V_1, V_2, ρ_1, and ρ_2). Therefore, six variables must be specified to solve the equations, providing that the equations are linearly independent. The number of variables can be reduced by utilizing Equations (3.20) and (3.21) along with the assumption that the delivered solids concentration is equal to the in-situ solids concentration. There will be error associated with this assumption for highly stratified slurries (delivered and in-situ solids concentration will be equal for non-settling slurries, but diverge as the flow becomes more stratified (Wilson et al., 2005)). Algebraic equations can be used to eliminate A_2, C_2, V_1, V_2, ρ_1, and ρ_2 from the model, leaving A_1, C_1, C and V.

$$A = A_1 + A_2 \tag{3.31}$$

$$V_2 A_2 = VA - A_1 V_1 \tag{3.32}$$

$$CAV = C_1 A_1 V_1 + C_2 A_2 V_2 \tag{3.33}$$

$$CA = C_1 A_1 + C_2 A_2 \tag{3.34}$$

$$\rho_1 = C_1 \rho_s + (1 - C_1)\rho_f \tag{3.35}$$

$$\rho_2 = C_2 \rho_s + (1 - C_2)\rho_f \tag{3.36}$$

This simplifies the model to:

$$\alpha(A_1, C_1, V, C)\frac{\partial C_1}{\partial t} + \beta(A_1, C_1, V, C)\frac{\partial A_1}{\partial t} + \gamma(A_1, C_1, V, C)\frac{\partial C_1}{\partial z} + \delta(A_1, C_1, V, C)\frac{\partial A_1}{\partial z} = \varepsilon(A_1, C_1, V, C)\frac{\partial C}{\partial t} + \epsilon(A_1, C_1, V, C)\frac{\partial V}{\partial t} + \zeta(A_1, C_1, V, C)\frac{\partial C}{\partial z} \quad (3.37)$$

where α, β, γ, δ, ε, ϵ, and ζ are 2 x 2 coefficient matrixes that are dependent upon process variables. The inputs are C and V, and the states are C_1 and A_1.

A step change in pressure moves down the pipe length when the bulk velocity is adjusted. This pressure change propagates at approximately 1000 m/s for water in a steel pipe (Paterson and Cooke, 2014; Wilson et al., 2005). Depending on the slurry, the speed is slightly higher or lower than the speed for water (Huggett, 1991). Due to the magnitude at which pressure changes move down the pipe, any bulk velocity change can be assumed to instantaneously affect the entire pipe length.

Furthermore, when the bulk velocity is adjusted, a new equilibrium between the layer variables must be reached. The advection-diffusion equation, otherwise known as the Schmidt-Rouse Equation, states that the gravitational and turbulent suspension forces are in equilibrium (Gillies and Shook, 1994):

$$\varepsilon_s \frac{dC}{dy} = V_\infty C \quad (3.38)$$

Since the two-layer model is only an approximation, it can be inferred from Equation (3.38) that the solids transfer between Layer 1 is in equilibrium with Layer 2. This means that slurry variables will not change as they move down the length of the pipe at steady-state (i.e., C_1 is not

changing with respect to time). It should be noted that Equation (3.38) is valid for low concentrations (Gillies and Shook, 1994); however, improvements can be made by using the hindered settling velocity as opposed to the terminal settling velocity (Gillies and Shook, 1994). For the purpose of this study, the layers are considered to be in equilibrium after the time it takes for particles to settle. This can be calculated using V_∞ and the pipeline diameter. Since the pipeline diameter is relatively small compared to the horizontal pipeline distance, the time it takes for the layers to be in equilibrium is negligible relative to the residence time in the pipe.

Equation (3.37) is quasi-linear, as the coefficients of the derivative terms vary with time, position, and the process variables (DuChateau and Zachmann 1989). From Equation (3.38) and the approximation that any change in velocity will instantaneously affect the entire pipeline, the coefficients of the derivative terms are assumed to not spatially vary at steady-state. Therefore, the coefficients in Equation (3.36) were approximated with their average values. This makes Equation (3.36) linear.

There are many methods to design controllers for systems described by PDEs (Ray, 1980). Early lumping approaches exploit the idea that PDEs can be approximated by ODEs along a discretized space (Ray, 1980). The number of discretized points and the approach to discretization (such as finite difference methods), may introduce inaccuracies into the model or require high-dimensional models (Moghadam, 2013). More efficient approaches depend on the type of PDE system. It is therefore necessary to analyze the model such that the PDE system can be classified. This study considers slurries primarily in the mining and oil sands industry. These slurries usually range from 180-300 μm median particle diameters and have solids concentrations greater than 0.35 (Schaan et al., 2007). Therefore, d_{50} was taken to be 225 μm and

C_t was taken to be 0.35 with a C_{rf} of 0.1. A pipeline inner diameter of 75.65 mm (to match pilot plant experimental tests to be performed in a future study) and a bulk velocity of 1.92 m/s (0.3 m/s above the deposition velocity) were chosen. These properties were provided to the SRC two-layer model to determine the steady-state values, which are reported in Table 1.

Table 1: Steady-state values from the SRC two-layer model with $C_r = 0.25$, $d_{50} = 225$ μm, D = 75.65 mm, and V = 1.92 m/s

Property	**Value**	**Unit**
C_1	0.22	volume fraction
C_2	0.38	volume fraction
A_1	3.1×10^{-3}	m^2
A_2	1.4×10^{-3}	m^2
V_1	2.29	m/s
V_2	1.11	m/s
ρ_1	1364	kg/m^3
ρ_2	1631	kg/m^3

Substituting the values from Table 1 into Equation (3.37) results in:

$$-1.22\frac{\partial C_1}{\partial t}+0.31\frac{\partial A_1}{\partial t}+15930\frac{\partial C_1}{\partial z}-5503\frac{\partial A_1}{\partial z}=-0.01\frac{\partial C}{\partial t}+0.01\frac{\partial C}{\partial z} \quad (3.39)$$

$$9.66\frac{\partial C_1}{\partial t}-3.34\frac{\partial A_1}{\partial t}-62668\frac{\partial C_1}{\partial z}+24669\frac{\partial A_1}{\partial z}=11.70\frac{\partial C}{\partial t}-6.35\frac{\partial V}{\partial t}-107.65\frac{\partial C}{\partial z} \quad (3.40)$$

The initial conditions for A_1 and C_1 can be steady-state values presented in Table 1, assuming that the pipeline is initially filled with "average" slurry. Additionally, if the boundary conditions are specified such that spatial position of zero corresponds to the outlet of a pump, then C_1 and A_1 can be calculated by assuming uniformly mixed slurry, which is further discussed in Chapter 5 and Figure 30. This means that A_1 can be equal to the total pipeline cross-section area, and C_1 can equal the total coarse solids volumetric fraction being inputted into the pipeline.

PDEs are often classified based on the general second-order equation:

$$a\frac{\partial^2 x}{\partial t^2}+b\frac{\partial^2 x}{\partial tz}+c\frac{\partial^2 x}{\partial z^2}+d\frac{\partial x}{\partial t}+e\frac{\partial x}{\partial z}+fx=g(x) \quad (3.41)$$

It should be noted that Equation (3.41) is not in the same form as the system represented by Equations (3.39) and (3.40). This is because PDE systems are more difficult to classify and solve than a single second-order PDE (Hoffman, 2001). Therefore, the single second-order PDE (i.e., Equation 3.41) will be explained before a system of first-order PDEs.

Second-order PDEs can be classified as hyperbolic, elliptic, or parabolic. Classification is determined from the sign of the discriminant (Hoffman, 2001 and DuChateau and Zachmann 1989):

$$b^2 - 4ac \tag{3.42}$$

If Equation (3.42) is negative, zero, or positive, the PDE is considered elliptic, parabolic, or hyperbolic, respectively. In a hyperbolic system, the PDEs have real distinct characteristics along which information can propagate (Hoffman, 2001). If the characteristic curves have the same sign, the information will propagate in one direction. If the signs are opposite, information flows in different directions (e.g., a counter-current heat exchanger) (Munusamy et al., 2014). Hyperbolic systems represent systems with advection as the main transport mechanism (Moghadam, 2013).

The method of characteristics is an analytical method that is commonly used to convert first order hyperbolic PDEs into ODEs (Rhee et al., 1986). This method uses "characteristic lines" that relate the time and space variables. Further information can be found in Jeffrey (2002), Shang (2002), and DuChateau and Zachmann (1989). For a system of equations, the intersection of the characteristic lines is called a "node," which represents the exact solution to the state variables at that specific time and spatial position (Munusamy et al., 2014). Since a node will rarely exist with three or more lines, this method is usually restricted to systems with only two characteristics (Munusamy et al., 2014). Figure 12 represents a system of two characteristic lines going in different directions. The lines are straight only when the PDE coefficients are constant. If the coefficients vary, the lines may no longer be parallel or become curved. All curves start at the initial point, z_0, and the number of nodes can be increased by decreasing the time spacing.

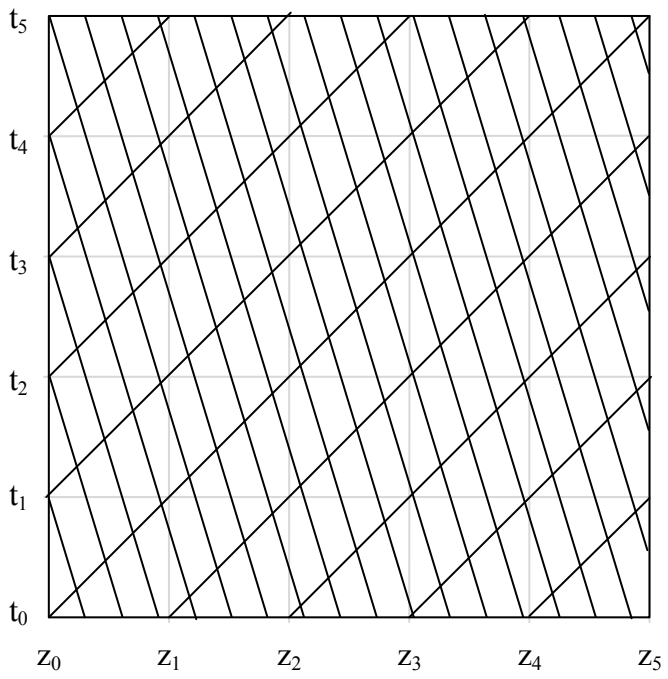

Figure 12: Characteristic grid for the Method of Characteristics

For a parabolic PDE, information propagates at infinite speed (Hoffman, 2001). They are associated with systems that have diffusion as a significant transport mechanism. The separation of variables technique can be used to turn the PDE into an infinite series solution (Jeffrey, 2003). An example of a general solution is:

$$x(z,t) = \sum_{n=1}^{\infty} C_n \sin\left(\frac{n\pi}{L} z\right) \exp(-\lambda_n{}^2 t) \tag{3.43}$$

where C_n represents coefficients found by the Fourier-sine series in Cartesian coordinates or the Fourier-Bessel series in cylindrical coordinates; L is the max z position; and λ_n are eigenvalues. The number of coefficients that one chooses will determine how many modes are included.

Further reading on this method can be found in Jeffrey (2003). If advection dominates over diffusion, this method may not be accurate unless a large number of modes are included (Shang et al., 2007).

In an elliptical system, information does not propagate in any preferred path (Hoffman, 2001). Therefore, the states at every point depend on the states at all other points (Hoffman, 2001). They can be solved analytically with the separation of variables technique, much like the parabolic case, and examples can be found in Bergman et al. (2011) and Budak et al. (1964).

The mass and momentum equations derived from the two-layer assumption resulted in a system of first-order PDEs. A single first order PDE is always hyperbolic (Hoffman, 2001). A system of first order PDEs with more than one dependent variable is not always hyperbolic (Hoffman, 2001; DuChateau and Zachmann 1989). Consider that all higher-order PDEs can be reduced to a system of first order equations (Fritz, 1982). This is achieved by introducing the dependent variables:

$$x = x_0 \tag{3.44}$$

$$\frac{dx}{dt} = x_1 \tag{3.45}$$

$$\frac{dx}{dz} = x_2 \tag{3.46}$$

Subsisting Equations (3.44)-(3.46) into Equation (3.41) results in a system of equations (Fritz, 1982), where x_0, x_1, and x_2 are dependent variables. The system is considered to be coupled because there will be more than one dependent variable in each of the equations (Hoffman, 2001). Therefore, there is potential for the system to be parabolic or elliptic, since the variables in the separate equations still rely on each other and are merely in a reduced form of Equation (3.41).

Consequently, a first order PDE system can be classified as hyperbolic, elliptic, or parabolic depending on the discriminant of the characteristic paths of the PDE system. A general coupled quasi-linear, first-order, nonhomogeneous PDE system with constant coefficients can be defined by (Hoffman, 2001):

$$\hat{a}\frac{\partial x_1}{\partial t} + \hat{b}\frac{\partial x_1}{\partial z} + \hat{c}\frac{\partial x_2}{\partial t} + \hat{d}\frac{\partial x_2}{\partial z} = \hat{e} \tag{3.47}$$

$$\hat{A}\frac{\partial x_1}{\partial t} + \hat{B}\frac{\partial x_1}{\partial z} + \hat{C}\frac{\partial x_2}{\partial t} + \hat{D}\frac{\partial x_2}{\partial z} = \hat{E} \tag{3.48}$$

The total derivatives of x_1 and x_2 are:

$$dx_1 = x_{1_t}dt + x_{1_z}dz \tag{3.49}$$

$$dx_2 = x_{2_t}dt + x_{2_z}dz \tag{3.50}$$

Equations (3.47)-(3.50) can be represented in matrix form:

$$\begin{bmatrix} \hat{a} & \hat{b} & \hat{c} & \hat{d} \\ \hat{A} & \hat{B} & \hat{C} & \hat{D} \\ dt & dz & 0 & 0 \\ 0 & 0 & dt & dz \end{bmatrix} \begin{bmatrix} x_{1_t} \\ x_{1_z} \\ x_{2_t} \\ x_{2_z} \end{bmatrix} = \begin{bmatrix} \hat{e} \\ \hat{E} \\ dx_1 \\ dx_2 \end{bmatrix} \tag{3.51}$$

The first derivatives can be uniquely solved by Cramer's rule unless the matrix of coefficients in Equation (3.51) is singular (Hoffman, 2001; Fritz, 1982). Setting the determinant of the coefficient matrix to zero yields the characteristic equation of the system:

$$\overline{A}(dz)^2 - \overline{B}(dz)(dt) + \overline{C}(dt)^2 = 0 \tag{3.52}$$

where:

$$\overline{A} = \left(\hat{a}\hat{C} - \hat{A}\hat{c}\right) \tag{3.53}$$

$$\overline{B} = (\hat{a}\hat{D} - \hat{A}\hat{d} + \hat{b}\hat{C} - \hat{B}\hat{c}) \tag{3.54}$$

$$\overline{C} = (\hat{b}\hat{D} - \hat{B}\hat{d}) \tag{3.55}$$

Equation (3.52) is a quadratic equation. Therefore, it can be solved via the quadratic formula:

$$\frac{dz}{dt} = \frac{\overline{B} \pm \sqrt{\overline{B}^2 - 4\overline{A}\overline{C}}}{2\overline{A}} \tag{3.56}$$

Equation (3.56) produces a family of curves. Each curve is a characteristic path of the PDE system, which defines how information propagates. The system of PDEs represented in Equations (3.47) and (3.48) has two characteristic paths. The quantity depends on the number of equations in the PDE system, and a more general approach can be found in DuChateau and Zachmann (1989). The discriminant of Equation (3.56) is:

$$\overline{B}^2 - 4\overline{A}\overline{C} \tag{3.57}$$

If the discriminant is positive, then the system is hyperbolic and the characteristic curves are real and distinct. If the discriminant is zero, the system is parabolic and Equation (3.56) has real and repeated values. If the discriminant is negative, the system is elliptic and Equation (3.56) has complex values (Hoffman, 2001).

The discriminant for the system represented by Equations (3.39) and (3.40) is -9.2×10^7, which implies that the system is elliptic. This is reasonable, as the steady-state dynamics dominate over the transient dynamics in the Equations (3.39) and (3.40), and elliptical systems are associated with steady-state equilibrium problems (Jeffrey, 2003). When higher-order hyperbolic or parabolic systems become independent of time at steady-state, they can become elliptic (Jeffrey, 2003). Additionally, steady-state flow of an incompressible liquid is known to be elliptic (Budak et al., 1964).

Recall for an elliptic PDE that the states at every point depend on the states at all other points (Hoffman, 2001). This is illustrated in Figure 13 for a slurry pipeline system. If the pipeline initially is loaded with slurry that has certain solids properties, and then a different slurry with

other solids properties is loaded, there will be two different vertical velocity profiles existing along the horizontal axis. It should be noted that the bulk velocity will be the same along the horizontal axis, but different solids sizes and concentrations will cause the solids to move at different axial and vertical velocities. This is illustrated in Figure 13 with two different vertical velocity profiles, where the second slurry is less stratified than the first slurry. This will cause the lower portion of the second slurry to move faster (dashed arrow) than the lower portion of the first slurry (solid arrow). The second slurry will reach the first slurry and mix. Initially, there will be a relatively short horizontal mixing region. As time increases, the mixing region will extend. As time goes to infinity, both slurries will have completely mixed and only one vertical velocity profile will exist in the pipeline. Therefore, the longer that the slurry is in the pipeline, the velocities and states (e.g., A_1, C_1) of all slurries in the pipeline will affect each other more.

In the two layer model, the vertical velocity profile is approximated by V_1 and V_2. Therefore, the pipeline illustrated in Figure 13 will be discretized vertically into a top and bottom section. While this PDE system alone cannot result in d_{50} and C_r predictions, there is value in solving it. It can predict V_1 and V_2 as opposed to using instrumentation (described in Chapter 5) and the resulting A_1, A_2, C_1, and C_2 can be used to make d_{50} and C_r predictions more accurate. Additionally, it can be used as a validation technique.

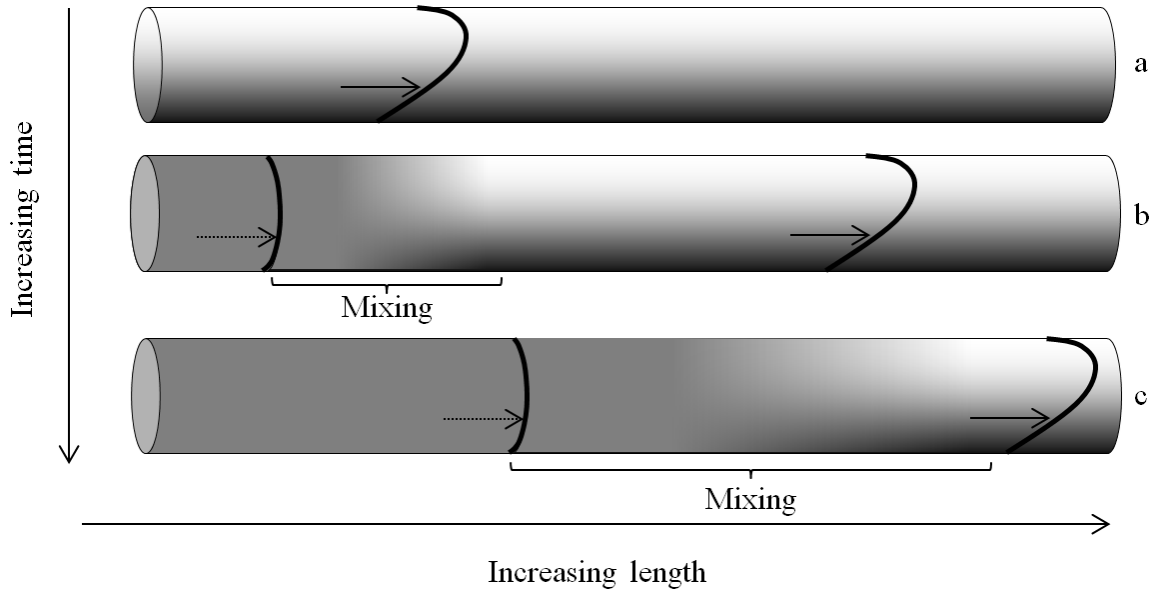

Figure 13: Two different slurries in the same pipeline with the same bulk velocity. At time (a), the pipeline has a highly stratified slurry that completely fills the length of the pipeline. At time (b), a less stratified slurry flows into the pipe. The velocity in the lower portion is greater (dotted arrow) than the original slurry (solid arrow). There is a mixing region. At time (c), the mixing length has extended.

4 Estimation of d_{50} and C_r

In this study, optimization is used to provide a best estimate of d_{50} and C_r, given pressure, velocity, and density information. The goal is to minimize the difference between the measured pressure gradient, P_{sensor}, and the estimated pressure gradient. The estimated pressure gradient is calculated using equations from the SRC two-layer model. The objective function includes the equation for the pressure gradient in Layer 1 (i.e. Equation (3.5)), which is a function of d_{50} and C_r. Constraints are included such that the pressure gradient in Layer 1 and Layer 2 are equal and that d_{50} and C_r do not take on unlikely values. The problem can be defined as:

$$\min_{d_{50},\, C_r} Z = \left(\frac{\tau_1 S_1 + \tau_{12} S_{12}}{A_1} - P_{sensor}\right)^2 \tag{4.1}$$

Subject to:

Equations (3.1)-(3.4), (3.9)-(3-21)

$$\frac{\tau_2 S_2 - \tau_{12} S_{12} + F_2}{A_2} - \frac{\tau_1 S_1 + \tau_{12} S_{12}}{A_1} = 0 \tag{4.2}$$

$$75\ \mu m \leq d_{50} \leq 650\ \mu m \tag{4.3}$$

$$0.3 C_t \leq C_r \leq C_t \tag{4.4}$$

Inequality (4.3) ensures that optimization provides a prediction of d_{50} to be within a reasonable range. The lower bound was chosen as fine particles are considered to be less than 74 μm (Shook et al., 2002), and C_r is defined as coarse particles (Shook et al., 2002). The upper bound was chosen to be higher than the largest particles commonly found in the oil sands industry, 300 μm (Schaan et al., 2007), in order to test a larger range of slurries. Inequality (4.4) ensures that C_r is not higher than the total measured concentration, but also ensures that the predicted particle size distribution (PSD) does not have more than 70% fines. This is required, because the SRC two-layer model assumes a narrow PSD. Since the objective function and constraints are not explicitly functions of d_{50} and C_r, the system of equations used for optimization must also contain Equations (3.1)-(3.4) and (3.9)-(3.21).

The inputs to the SRC two-layer model are Q, d_{50}, C_r, C_{max}, k, D, ρ_s, ρ_f, and μ_f. Since the only variables that are being predicted are d_{50} and C_r, the remaining inputs must be specified. Furthermore, the pressure gradient in the pipeline, P_{sensor}, and the velocities of the two layers, V_1 and V_2, must also be specified. The SRC two-layer model uses semi-empirical ODEs to calculate the concentration profile, and uses the concentration at a normalized height position of 0.15 as the value for C_2 (Gillies and Shook, 1994). If V_1 and V_2 are specified, then C_2 can be solved with algebraic mass and momentum balances. For the purposes of this study, P_{sensor}, V_1, V_2, Q, and p_m will be determined using the SRC two-layer model. Normally, they would be supplied by instrumentation, as detailed in Chapter 5. The parameters D, C_{max} and ρ_s are provided by operations personnel, as they are not expected to change during pipeline operation. The carrier fluid properties, μ_f and p_f, are determined as a function of C_t. Therefore, additional equations must be included to calculate μ_f and p_f. The fines concentration is calculated via Equation (3.4), which can then be used to find μ_f with a commonly used correlation for the design of slurry

pipelines (Smith, 2013). Equation (4.5) was correlated using mature fine tailings for C_t samples of 0.1 to 0.3 (Shook et al., 2002):

$$\mu_f = \mu_L \exp(12.5 C_f) \tag{4.5}$$

There are many correlations for carrier fluid viscosity available (Smith, 2013). The correlation used should most accurately reflect the slurry in the pipeline. The total solids concentration can be determined from ρ_m:

$$C_t = \frac{\rho_m - \rho_L}{\rho_s - \rho_L} \tag{4.6}$$

The remaining variables that cannot be provided by instruments or operations are d_{50} and C_r. The variables that must be provided to the estimation method and the decision variables are summarized in Table 2:

Table 2: Variables required for the optimization model

Provided Variables	Decision Variables
$\Delta P/\Delta z$ (P_{sensor})	C_r
V_1	d_{50}
V_2	
Q	
ρ_m	
ρ_s	
D	
C_{max}	
μ_L	
ρ_L	

The SRC two-layer model has three main assumptions: the flow is turbulent, the pipeline is horizontal, and d_{50} is the size of all of the coarse particles in the slurry (Saskatchewan Research Council, 2014). It is acceptable to assume that the flow is turbulent, as laminar flow will cause deposition. It will also be assumed that the estimation method is for horizontal pipelines only. Additionally, it is inaccurate to assume d_{50} represents all of the coarse particles, because d_{50} is a measure of the median particle size in a particle size distribution (PSD). Consequently, this

model works best for narrow PSDs. Prediction errors may result for broad PSDs. In this case, d_{50} should be adjusted accordingly, as the largest particles have the most influence on V_c predictions (Saskatchewan Research Council, 2014).

4.1. Problem Solution

In numerical optimization, an objective function is iteratively improved by systematically changing the decision variables. The goal is to minimize or maximize the objective function, which is a function of the decision variables. The objective function can be subject to constraints. Equality constrains usually represent a system's behavior and inequality constraints usually represent physical limitations on the system.

For scalar, deterministic, and continuous problems, optimization methods are generally split into linear programming or nonlinear programming (Nocedal and Wright, 2006). Linear programing is used when the objective function, constraints, and the equations in the problem are entirely linear. Nonlinear programming is used when the objective function, constraints, or any equation in the problem is nonlinear (Griva et al., 2012). Nonlinear programming will be used since the SRC two-layer model is nonlinear. Additionally, since there are two decision variables and three constraints, the problem is classified as a constrained nonlinear multivariate optimization problem.

There are many different types of nonlinear programs. The objective function in this study is continuous, and a branch of nonlinear program types that are well-suited for continuous functions are gradient methods. Gradient methods are faster and more accurate than methods that

do not use derivatives (Edgar et al., 2001) and are the base of most of the widely used nonlinear optimizers used presently (Edgar et al., 2001).

The gradient is defined as a vector of first derivatives of the objective function with respect to each individual decision variable. For this problem, the gradient is:

$$\nabla Z = \left[\frac{dZ}{dd_{50}} \quad \frac{dZ}{dC_r}\right] \tag{4.8}$$

The objective function will decrease the fastest in the direction of the negative gradient. If the gradient is equal to 0, then a stationary point, or a relative maxima or minima, has been found (Edgar et al., 2001).This is one necessary condition to prove that an optimum is found. Another condition is that the Hessian is positive definite (for a minimization problem) or negative definite (for a maximization problem) at an optima (Edgar et al., 2001). The Hessian is a matrix of second order derivatives of the objective function with respect to the decision variables. It represents the rate of change of the first derivatives, and is used as an indicator of whether the slope of the first derivative is decreasing (negative second derivative) or increasing (positive second derivative). In this problem, the Hessian is defined as:

$$H = \nabla^2 Z = \begin{bmatrix} \frac{\partial^2 Z}{\partial d_{50}^2} & \frac{\partial^2 Z}{\partial d_{50}\,\partial C_r} \\ \frac{\partial^2 Z}{\partial d_{50}\,\partial C_r} & \frac{\partial^2 Z}{\partial C_r^2} \end{bmatrix} \tag{4.9}$$

The eigenvalues, λ, of the Hessian can be calculated by finding the roots of the characteristic equation (Forbes and Aksikas, 2010b):

$$|\lambda I - H| = 0 \tag{4.10}$$

where I is an nxn identity matrix, given that n is the size of the Hessian. The eigenvalues are a measure of scaling corresponding to a certain direction, and can be used to describe the Hessian.

These necessary and sufficient conditions can be developed via a second order Taylor expansion (Edgar et al., 2001). Let f(x) be a nonlinear function, x is a variable, and x* is the value of x at the minimum value of f(x). The Taylor expansion about x* is:

$$f(x) = f(x^*) + \nabla f(x)|_{x=x^*}(x - x^*) + \frac{1}{2}\nabla^2 f(x)|_{x=x^*}(x - x^*)^2 + \cdots \tag{4.11}$$

Since f(x*) is a minimum, the gradient at this point will be equal to zero. Additionally, f(x) will be greater than f(x*). Therefore, there needs to be an additional positive value on the right-hand-side for the equation to be valid. Since a quadratic term is always positive, the Hessian must also be positive. Likewise, if it was a maximization problem, the Hessian must be negative for the equation to be valid. Figure 14 shows a function with a maximum and minimum, and its corresponding first and second derivatives.

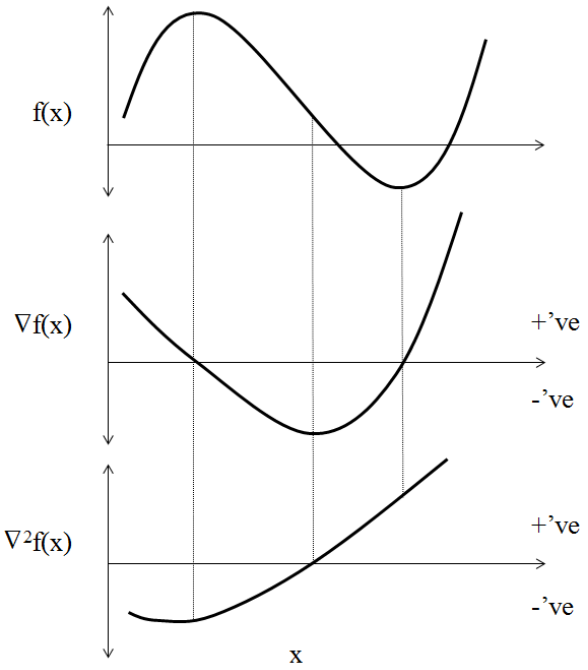

Figure 14: A function with a maximum and minimum, the first derivative of the function, and the second derivative of the function.

Determining if the gradient is zero and the Hessian is positive or negative is not enough to prove if a global maximum or minimum has been found. If a function is convex, the solution calculated by the optimization model is guaranteed to be a global solution (Edgar et al., 2001). A convex function can be defined as a subspace that contains any line segment joining any two points within the subspace (Dullerud and Paganini, 2000). Optimization of a nonconvex function may result in local solutions. Figure 15 represents a convex and nonconvex set.

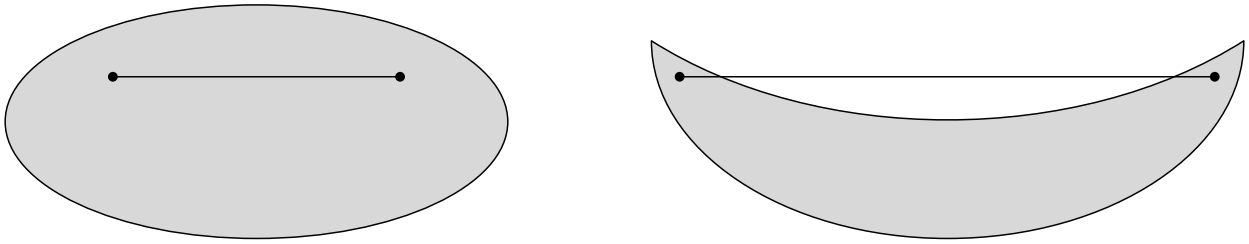

(a) (b)

Figure 15: Convex (a) and nonconvex (b) sets (Dullerud and Paganini, 2000)

A function can be determined to be convex if the eigenvalues of the Hessian are positive (Edgar et al., 2001). Since the Hessian is analytically unsolvable for this problem, the subspace of the function will be determined graphically, as seen in Figure 16. This is possible because there are only two variables, otherwise approximate Hessian calculations could be used to determine convexity.

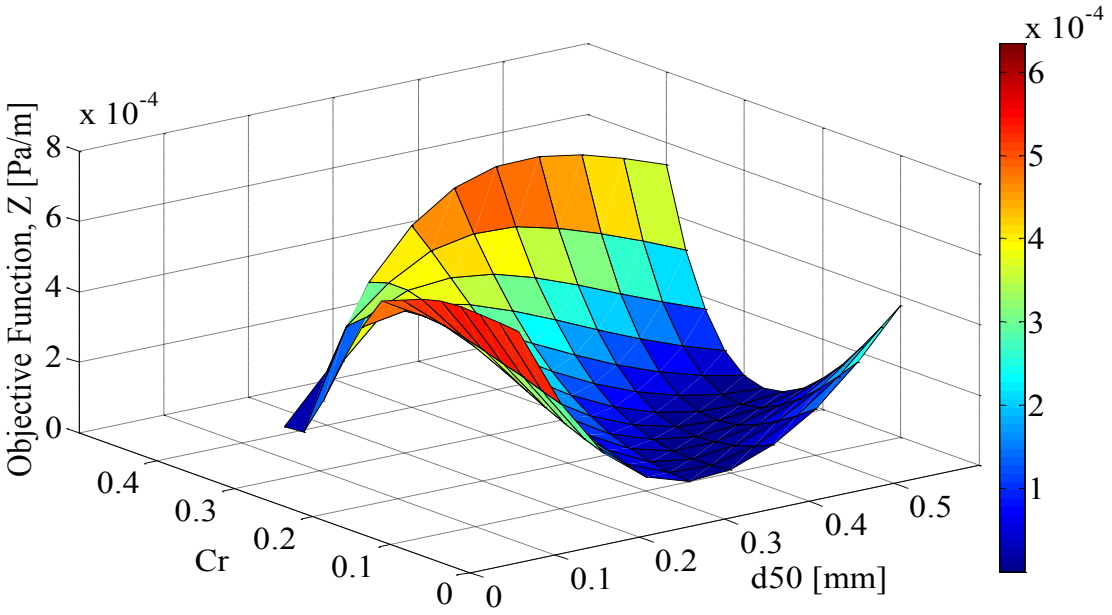

Figure 16: Objective function as C_r and d_{50} vary for P_{sensor} equal to 1632 Pa/m

In Figure 16, C_r and d_{50} were scaled, which will be described later in this section. The value for P_{sensor} was 1632 Pa/m, and the corresponding V_1 and V_2 were held constant as d_{50} and C_r were varied. This represents how the optimization algorithm finds a solution. It does not represent how slurries behave in reality. Figure 16 shows that this function is not convex. This means that it is possible to have local solutions. Therefore, the starting point is very important, as described below. Also, it can be seen that even though the problem is scaled, there is still a region of very low curvature for d_{50}. This may result in insensitivities to d_{50} and prediction errors.

The method described above has partially explained the steepest-decent optimization algorithm, and introduces the basic concept behind gradient-based nonlinear programming. This method is very sensitive to scaling (Edgar et al., 2001); therefore, it will not be used.

Many types of nonlinear programs use the Hessian to modify the direction of change for variables. This is more efficient (i.e., requires fewer iterations) than models that only use gradients (Edgar et al., 2001). For this problem, calculating the Hessian is as complicated as back-calculating the SRC two-layer model analytically. Therefore, nonlinear programming models that approximate the Hessian will be used. Approximating the derivatives may decrease accuracy and increase computational difficulty (Edgar et al., 2001).

The interior-point optimization method was chosen as it works well for problems with scaling issues, nonlinear constraints, and for nonconvex problems (Nocedal and Wright, 2006; Bertsekas, 1999). Additionally, it can be computationally efficient (Bertsekas, 1999).

Interior-point methods move through the feasible region toward the optimum and can be classified as a feasible path method. Active set methods move around the boundary of the feasible region (such as in linear simplex methods). These two methods are illustrated in Figure 17. Additionally, there are also infeasible path methods that allow constraint violations (such as with some penalty methods) (Nocedal and Wright, 2006).

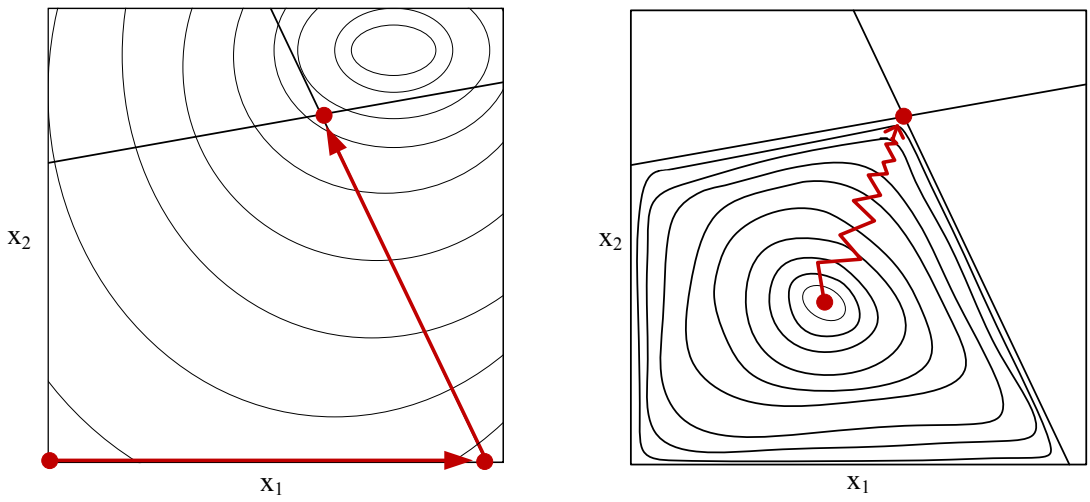

Figure 17: Optimization problem contours, with straight lines as constraints. (a) Active set method. (b) Feasible path method (Hedengren, 2104 and Bertsekas, 1999)

In interior-point methods, the constrained optimization problem is converted into an unconstrained problem by merging the constraints and the objective function into a new objective function (Bertsekas, 1999). To ensure that the decision variables are within the feasible region, the constraint is incorporated into a natural logarithm term in the objective function, which creates a barrier function. For example, a general constrained optimization problem can be written as (Nocedal and Wright, 2006):

$$\min_{\mathbf{x}} f(\mathbf{x}) \tag{4.12}$$

$$\text{subject to } g(\mathbf{x}) \leq 0 \tag{4.13}$$

where **x** is a vector of variables. Applying the interior-point method turns the problem into:

$$\min_{\mathbf{x}}\{f(\mathbf{x}) - \ln[-g(\mathbf{x})]\} \tag{4.14}$$

As g(x) approaches zero, the natural log will approach negative infinity. This adds a very large term to the objective function. Since the objective function is being minimized, the decision variables will be chosen to be far away from the barrier (the limit imposed by constraints), which may not accurately reflect the true solution. Therefore, a barrier parameter, r, is used as a multiplier for the barrier function.

$$\min_{\mathbf{x}}\{f(\mathbf{x}) - \mathbf{r}\ln[-g(\mathbf{x})]\} \tag{4.15}$$

The barrier parameter is a positive scalar, and as it approaches zero, Equation (4.15) approaches the original objective function as the barrier function's weight is decreased. As a result, the decision variables are allowed to move closer to the barrier (Nocedal and Wright, 2006). Figure 18 represents the interior-point method with decreasing values of r.

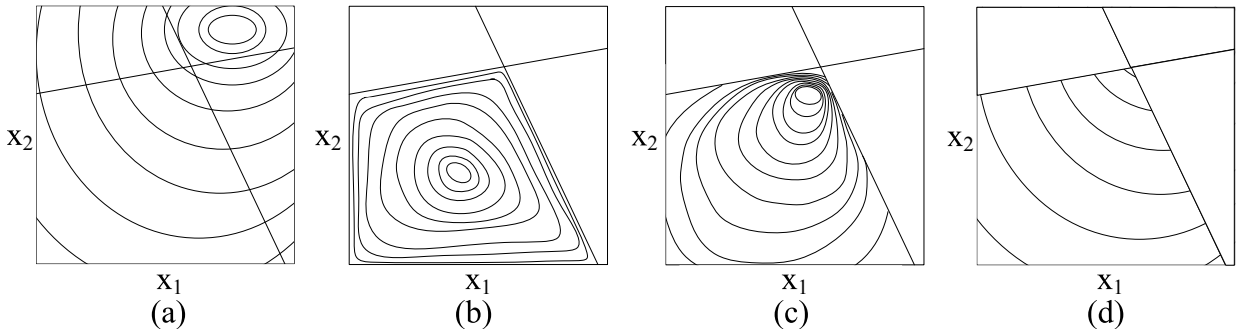

Figure 18: Interior point method. (a) Original Objective function. (b) Interior-point objective function with a high barrier parameter value. The natural log function dominates and the decision variables are far away from the real optimal. (c) Interior-point objective function with a smaller barrier parameter value than in (b). Decision variables are closer to the real optimal. (d) Interior-point objective function with the barrier parameter value infinitely small such that the contours match the original objective function in (a) (Hedegren, 2014 and Bertsekas, 1999).

The barrier parameter is chosen by solving Equation (4.15) with a positive starting value. Equation (4.15) is repeatedly solved after the barrier parameter is decreased (monotonically) toward zero. The best way to decrease the barrier parameter is an area of active research (Byrd et al., 2000), and some algorithms are presented in Nocedal and Wright (2006). Often, the barrier parameter is changed faster near the solution. It should be noted that if r is decreased too slowly, then many iterations may be required, but if it is decreased too quickly, then the objective function may converge to an incorrect answer (Nocedal and Wright, 2006).

The MATLAB function *fmincon* was used to apply the interior-point nonlinear program to the SRC two-layer model. It approximates the Hessian with a dense quasi-Newtonian approximation

(The MathWorks, Inc., 2014a). The initial barrier parameter is 0.1. The default termination criteria, convergence tolerances, and step lengths were used. The algorithm terminated after the difference between the objective function value at the previous and current best point was less than $1x10^{-6}$ and the constraint was satisfied within $1x10^{-6}$. The initial starting points are given in Table 3:

Table 3: Starting point of optimization model

$\mathbf{d_{50}}$	$\mathbf{C_r}$
225 μm	C_t*0.9

Often, several starting points are used to avoid local solutions; however, changing the starting point had no difference on the prediction results as long as the slurry was not highly stratified. From Figure 16, it can be seen that as long as the C_r starting point was not too large, the solution should converge to the d_{50} low curvature region. The upper bound in Constraint (4.4) also prevented local solutions as C_r was not allowed to be higher than C_t.

The units for d_{50}, C_r, and pressure gradient in the SRC two-layer model are meters, volume fraction, and Pa/m, respectively. Their values vary over 6 orders of magnitude. This means changes to C_r will result in larger changes to the objective function compared to changes in d_{50}. Scaling can prevent this issue (Nocedal and Wright, 2006). When problems are scaled, the eigenvalues of the Hessian, Equation (4.10), are approximately of the same magnitude (Bertsekas, 1999). This makes the contours of the objective function concentric circles (Forbes

and Aksikas, 2010b). This can be important for certain optimization methods, because the gradient (Equation (4.8)) will always point toward an optimum (Edgar et al., 2001). If the problem is unscaled, the contours of the objective function are elliptical, because one variable "stretches" the function. When this happens, the gradients are unlikely to pass through the optimum (Edgar et al., 2001). Additionally, ridges in the function might be created (Edgar et al., 2001). Ridges indicate that one variable will change quickly, but the other will become "trapped" where changing it has little effect on the objective function. The units of the decision variables and objective function were changed to have values with a magnitude from 0 to 1 such that the problem was well-scaled (Nocedal and Wright, 2006). The units of C_r remained the same, and the units for d_{50} and pressure gradient were changed to millimeter and Pa/mm, respectively. Once a result was attained, the units were converted back.

After all of the simulations were performed, it was found that there was a consistent bias in the estimations. Therefore, a constant of 100 μm was subtracted from all d_{50} estimations, and a constant of 0.04 was added to all C_r estimations. Furthermore, it was found that predictions for d_{50} were at the upper bound for known values of d_{50} less than 125 μm. For these slurries, the optimization algorithm was run again without scaling. Additionally, the optimization algorithm consistently returned local solutions as the concentration and particle size increased. If the objective function was greater than $1x10^{-7}$, the optimization function was run again without Constraint (4.2).

4.2. Simulation Results

The optimization model was run for C_r values of 0.1, 0.125, 0.2, 0.225, 0.3, 0.325, 0.35, and 0.4, with d_{50} values between 75 to 625 μm with 25 μm intervals. The diameter of the pipe was chosen to be 75.65 mm to match experimental tests to be carried out in the future. The known variables in Table 2 were calculated by using C_r and d_{50} values in the SRC two-layer model. The flowrate, Q, was chosen to be 0.0135 m^3/s, which is in heterogeneous flow. Inputs into the SRC two-layer model had a C_f value of 10% of C_t. The parameter values of C_{max} and ρ_s were taken to be 0.635 and 2650 kg/m^3, respectively, and the liquid carrier was water.

A percent error was calculated based on:

$$\% \text{ error} = \frac{\text{abs}(\text{predicted} - \text{actual})}{\text{actual}} \text{x}100 \tag{4.15}$$

Figure 19 to 21 show the predicted values of C_r, d_{50}, and pressure gradient, respectively, plotted with the SRC two-layer model values as a function of run number for known C_r values of 0.1, 0.125, 0.2, and 0.225. Run number was chosen as the x axis as C_r and d_{50} were predicted simultaneously. The predictions for C_r had an average error of 6.0%. The predictions for d_{50} had an average error of 8.9%. Runs 48 and 71 had d_{50} and C_r predictions with more error than other run predictions. This may be due to local minimums as 100 μm is close in size to fine particles. For known d_{50} values of approximately 550 μm and higher, the predicted d_{50} values were 550 μm and the C_r predictions were lower than other C_r predictions. This is most likely due to Coulombic friction introducing many peaks and ridges into the objective function. Consequently,

the optimization algorithm can become stuck in local solutions. All other runs have negligible pressure gradient prediction errors except for these runs. This supports the possibility that the optimization algorithm found a local solution.

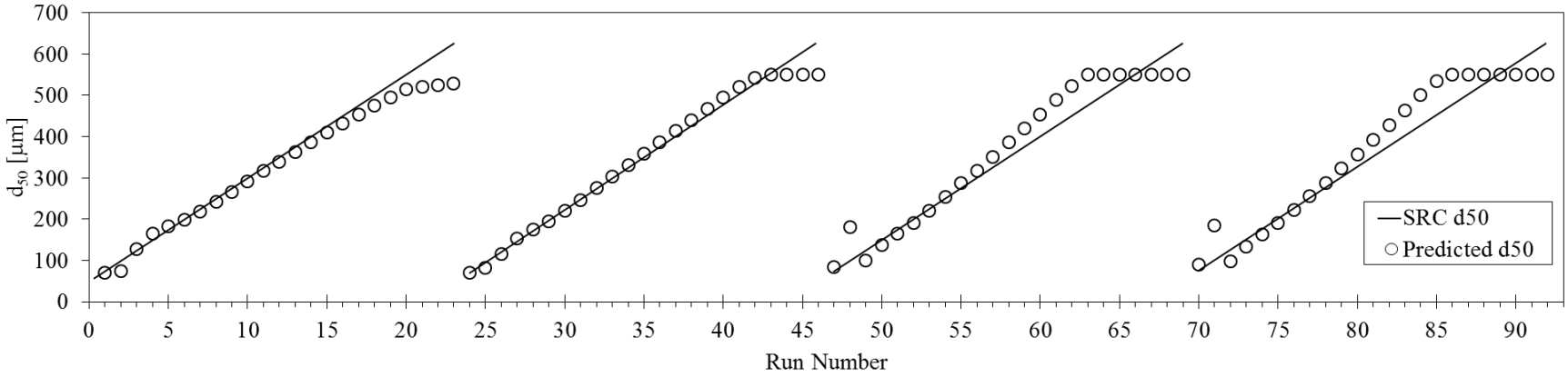

Figure 19: Predicted d_{50} for known C_r values of 0.1, 0.125, 0.2, and 0.225 with known values of d_{50} from 75 to 625 µm

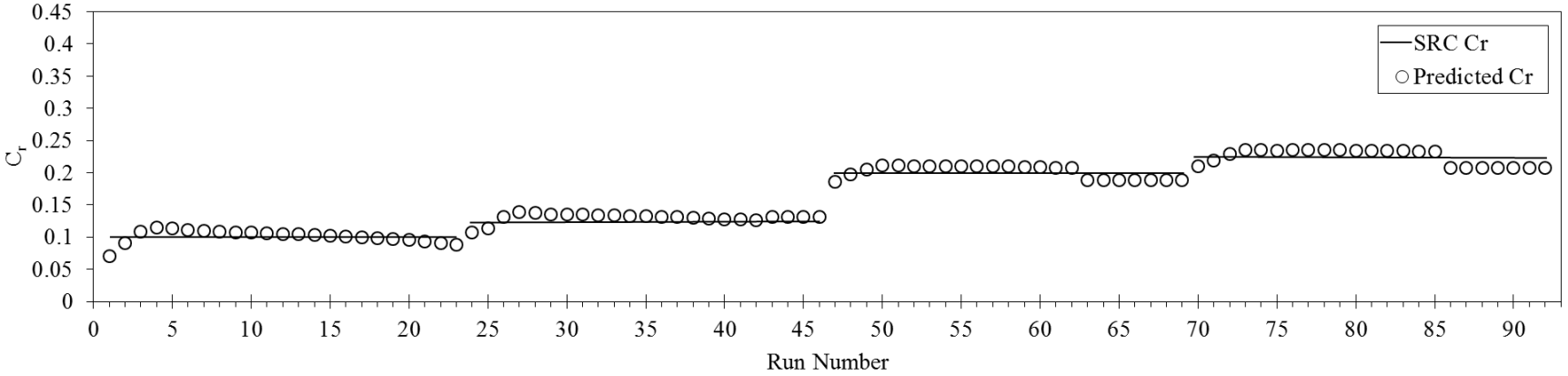

Figure 20: Predicted C_r for known C_r values of 0.1, 0.125, 0.2, and 0.225 with known values of d_{50} from 75 to 625 µm

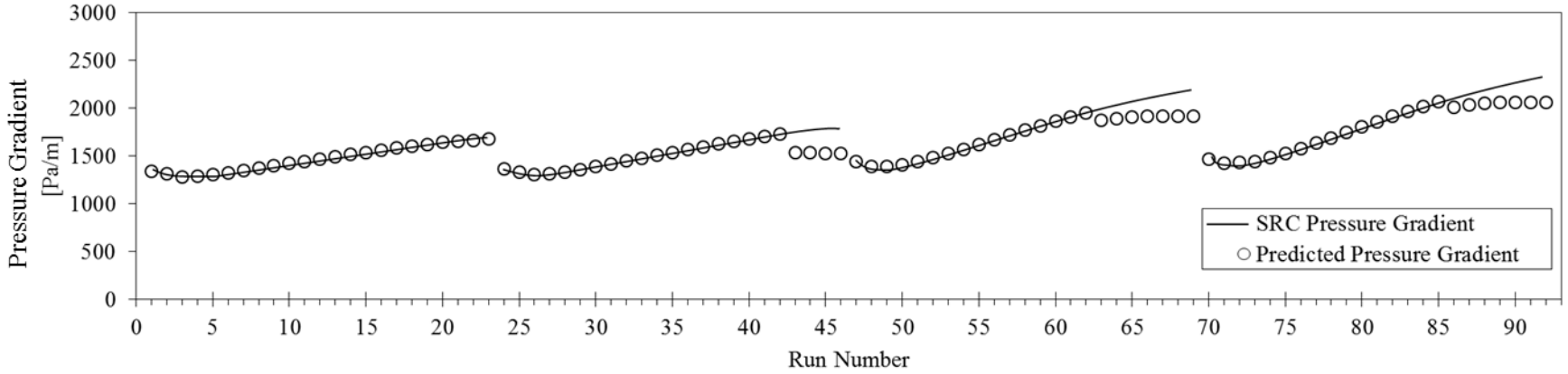

Figure 21: Predicted pressure gradient for known C_r values of 0.1, 0.125, 0.2, and 0.225 with known values of d_{50} from 75 to 625 µm

Figure 22 to 24 show the predicted values of C_r, d_{50}, and pressure gradient, respectively, plotted with the SRC two-layer model values as a function of run number for known C_r values of 0.3, 0.325, 0.35, and 0.4. Run number was chosen as the x axis as C_r and d_{50} were predicted simultaneously. Predictions for C_r had an average error of 2.3%. Predictions for d_{50} had an average error of 18.4%. Runs 94, 117, and 140 had d_{50} predictions and C_r predictions with more error than the rest of the predictions. It is suspected that the optimization algorithm matched the pressure gradient with a smaller concentration of larger particles (i.e. the optimization algorithm found a local optimum). For known d_{50} values of approximately 550 μm and higher, the d_{50} predictions were 550 μm. This corresponds to the upper bound without modifications after optimization. For these runs, the optimization algorithm was run again without Constraint (4.2). This causes d_{50} predictions to have a sharp spike around 550 μm. It is suspected that removing the constraint improves the predictions where the optimization algorithm may become stuck in a local optimum. This modification did not improve predictions for runs with C_r values of 0.3. The predicted pressure gradient also has error for runs where the constraint was removed. This indicates that removing the Coulombic friction constraint introduces error into the pressure gradient prediction.

For all runs, the average error for d_{50} and C_r were 13.6% and 4.2%, respectively. Therefore, it is possible to predict slurry properties using the SRC two-layer model and an interior-point optimization algorithm. The estimation method did not result in perfect predictions, and errors were caused by Coulombic friction induced local optimums, and slurries with small d_{50} having equal pressure gradients with a smaller concentrations of larger particles. It may be possible to reduce errors with additional optimization techniques, such as multiple starting points.

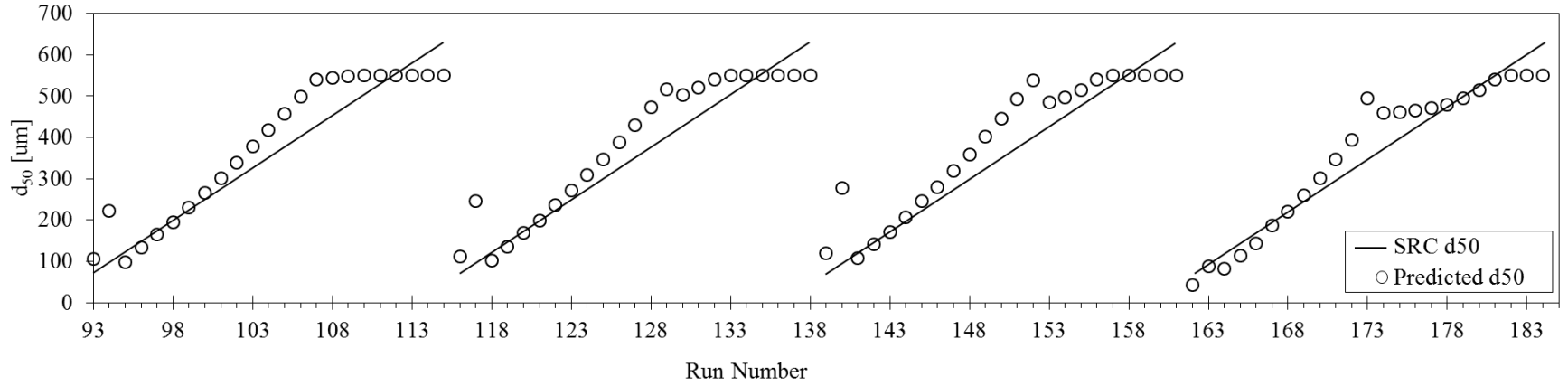

Figure 22: Predicted d_{50} for known C_r values of 0.3, 0.325, 0.35, and 0.4 with known values of d_{50} from 75 to 625 µm

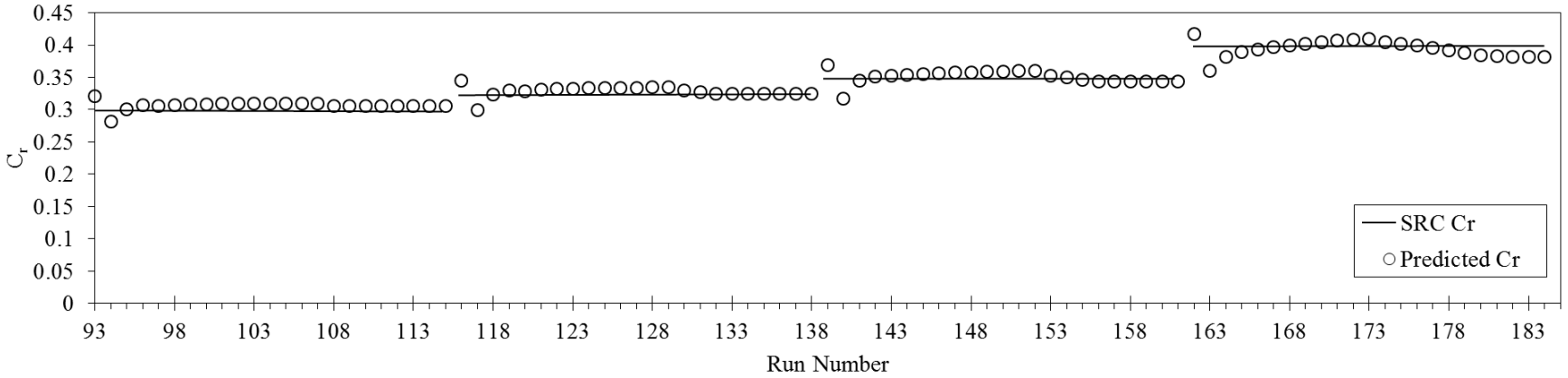

Figure 23: Predicted C_r for known C_r values of 0.3, 0.325, 0.35, and 0.4 with known values of d_{50} from 75 to 625 µm

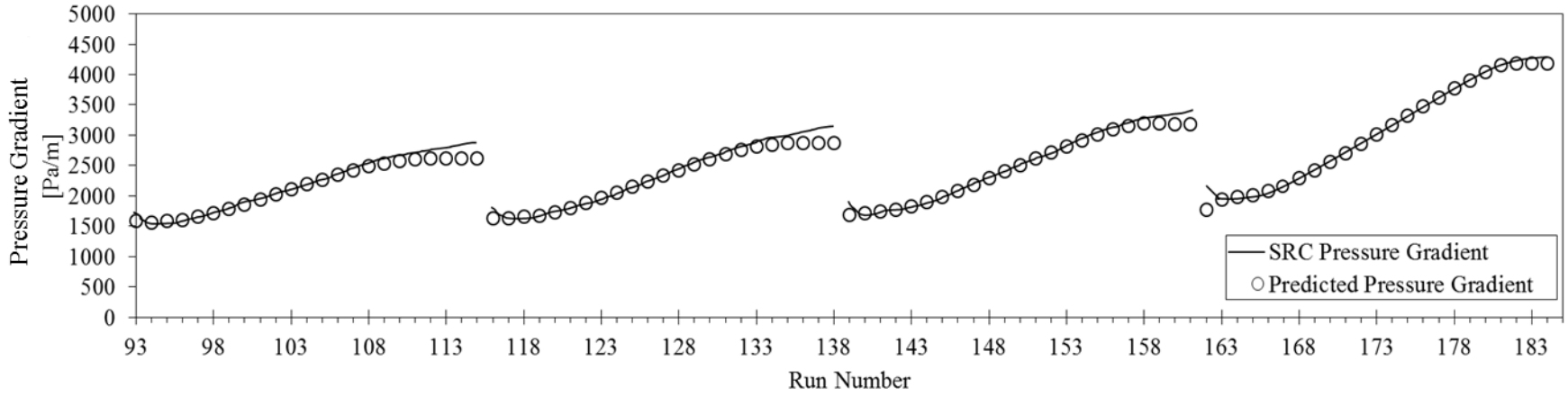

Figure 24: Predicted pressure gradient for known C_r values of 0.3, 0.325, 0.35, and 0.4 with known values of d_{50} from 75 to 625 µm

4.3. Discussion

Figure 25 represents the calculated deposition velocity using known and predicted d_{50} and C_r values for known C_r values of 0.1, 0.125, 0.2, and 0.225. Predicted V_c values were calculated by using the d_{50} and C_r values from the estimation method, and known V_c values were calculated by using the d_{50} and C_r values that were used as inputs in the SRC two-layer model. The error was 4.8%. Runs 48 and 71 had error associated with V_c due to the error in predicted d_{50} and C_r. Runs 63-69 and 86-91 corresponded to the runs with d_{50} predictions of 550 μm and C_r predictions less than the known C_r values. These errors caused V_c predictions to be lower than the V_c known values.

Figure 26 represents the calculated deposition velocity using known and predicted d_{50} and C_r values for known C_r values of 0.3, 0.325, 0.35, and 0.4. Predicted V_c values were calculated by using the d_{50} and C_r values from the estimation method, and known V_c values were calculated by using the d_{50} and C_r values that were used as inputs in the SRC two-layer model. The error was 6.3%. Runs 93, 116, and 139 had error associated with V_c, because the predicted C_r was higher than the known C_r. Runs 94, 117, and 140 had error associated with V_c due to the error in predicted d_{50} and C_r. Runs 152 and 173 had higher V_c predictions than other predictions due to the modifications applied for high concentration and large particle sizes.

The error from the predicted d_{50} and C_r values propagated through V_c calculations and gave V_c predictions a 5.5% average error. Even with error, the predicted V_c can still be used to calculate a suggested velocity, described in Chapter 5.

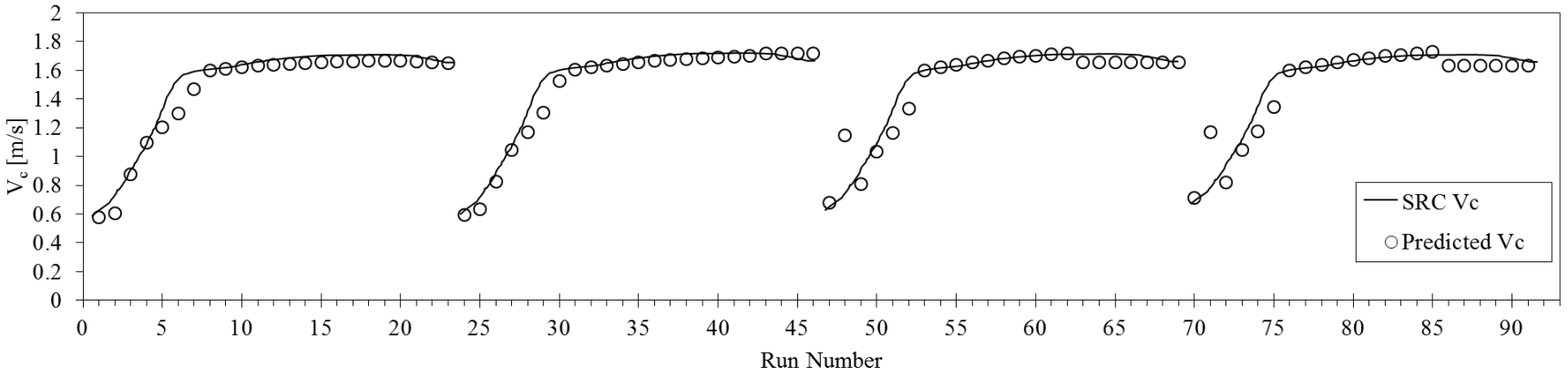

Figure 25: Predicted deposition velocity for known C_r values of 0.1, 0.125, 0.2, and 0.225 with known values of d_{50} from 75 to 625 µm

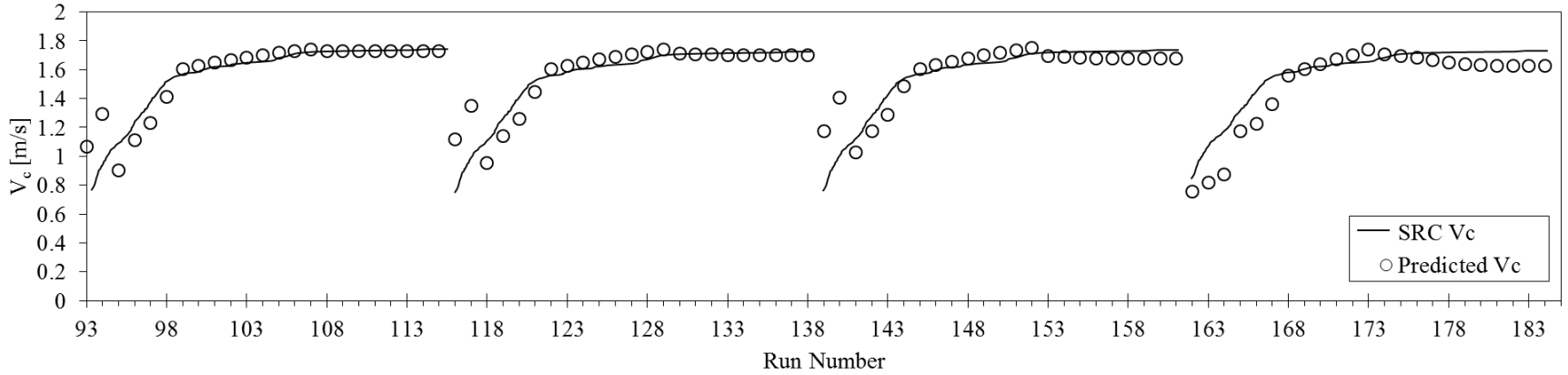

Figure 26: Predicted deposition velocity for known C_r values of 0.3, 0.325, 0.35, and 0.4 with known values of d_{50} from 75 to 625 µm

Figure 27 and Figure 28 represent the calculated SEC using known and predicted d_{50} and C_r values versus bulk velocity. The known and predicted minimum SEC locations are also illustrated. The known minimum SEC was calculated graphically from the known SEC curve, and the predicted minimum SEC was calculated from multiplying the predicted V_c by a safety factor of 1.15 (Hashemi, 2014b). Figure 27 illustrates slurry with known values of $C_r = 0.35$ and $d_{50} = 225$ μm (the equivalent predicted values are from run 145) to represent average slurry conditions in the oil sands industry (Schaan et al., 2007). Figure 28 shows slurry with known values of $C_r = 0.125$ and $d_{50} = 500$ μm (the equivalent predicted values are from run 41) to represent a change in conditions from the average slurry. For average conditions, the predicted SEC has an average 6.6% error. For the 500 μm slurry, the predicted SEC had an average error of 15.8%. Both trends were predicted accurately. The predicted minimum SEC gave a conservative estimate. The velocity corresponding to the minimum predicted SEC was 0.16 m/s higher than the velocity corresponding to the known minimum SEC for the average slurry, and 0.7 m/s for the 500 μm slurry. This is reasonable, as velocity contingency factors are used in industry (Thomas, 2014), and a safety factor of 1.15 was applied (Hashemi, 2014b). If the minimum SEC was calculated graphically from the predicted SEC graph, the predicted minimum SEC would be in close agreement to the actual minimum SEC.

Error in d_{50} and C_r predictions propagate through calculations and will also introduce error into V_c and SEC predictions. The SEC prediction trends matched the known SEC trends, and the minimum SEC could be predicted graphically with good agreement to the known minimum. The minimum SEC could also be predicted with predicted V_c values; however the prediction was conservative as a safety factor was used. This is acceptable as pipelines are operated with a velocity contingency factor (Thomas, 2014).

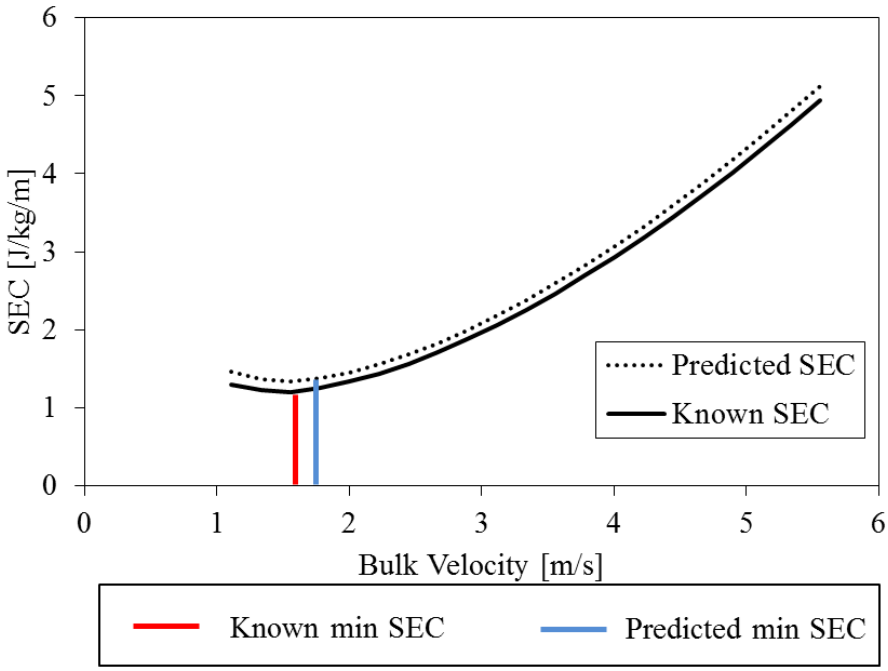

Figure 27: Predicted and known SEC versus bulk velocity for C_r=0.35 and d_{50}=225 µm

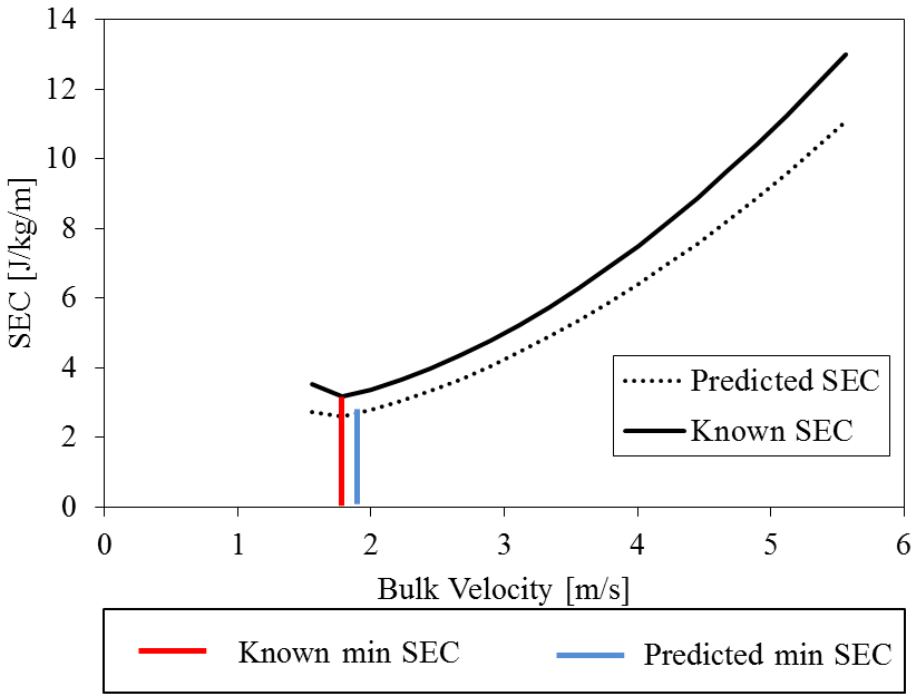

Figure 28: Predicted and known SEC versus bulk velocity for C_r=0.125 and d_{50}=500 µm

5 Implementation

In this section the instruments necessary for d_{50} and C_r prediction on an actual pipeline are detailed, which includes the placement of instruments and the frequency of data collection. Instruments will be required to transmit pressure gradient, velocities, and density measurements to a computing system. The instruments and their uses can be seen in Table 4.

Table 4: Inputs required for d_{50} and C_r prediction and their respective instruments (Fredagsvik, 2014; Gillies, 1991)

Input into Estimation Method	**Provided by Instrumentation**	**Dynamics**
Pressure Gradient	Pressure transducers	Fast
Top and Bottom Velocities	Velocity Profiler	Fast
Overall Flow Rate	Flowmeter	Fast
Mixture density	Mixture densitometer	Slow

A data acquisition system will also be required to convert the signals from the instruments into a form that is useful for a computer. Data should be collected at an appropriate frequency and filtered to reduce noise. Shannon's sampling theorem states that a signal must be sampled at least twice per period, otherwise important information may not be recovered (Seborg et al., 2011). A guideline is to sample at five times Shannon's minimum rate. Since the optimization model only

takes seconds to run, it is suggested to run the optimization model every minute. This allows the data from the instruments to be filtered every 60 seconds. Note that this sample time may or may not satisfy Shannon's sampling theorem and should be checked upon implementation. Additionally, filtering will cause information about the fast dynamics to be lost. This is acceptable, because changes to the pressure gradient (and thus the bulk velocity) propagate at approximately 1000 m/s (Wilson et al., 2005) and will be assumed to be instantaneous. Furthermore, transient conditions are not required to be captured as the estimation method treats the inputs at steady state. The following block diagram in Figure 29 illustrates the system.

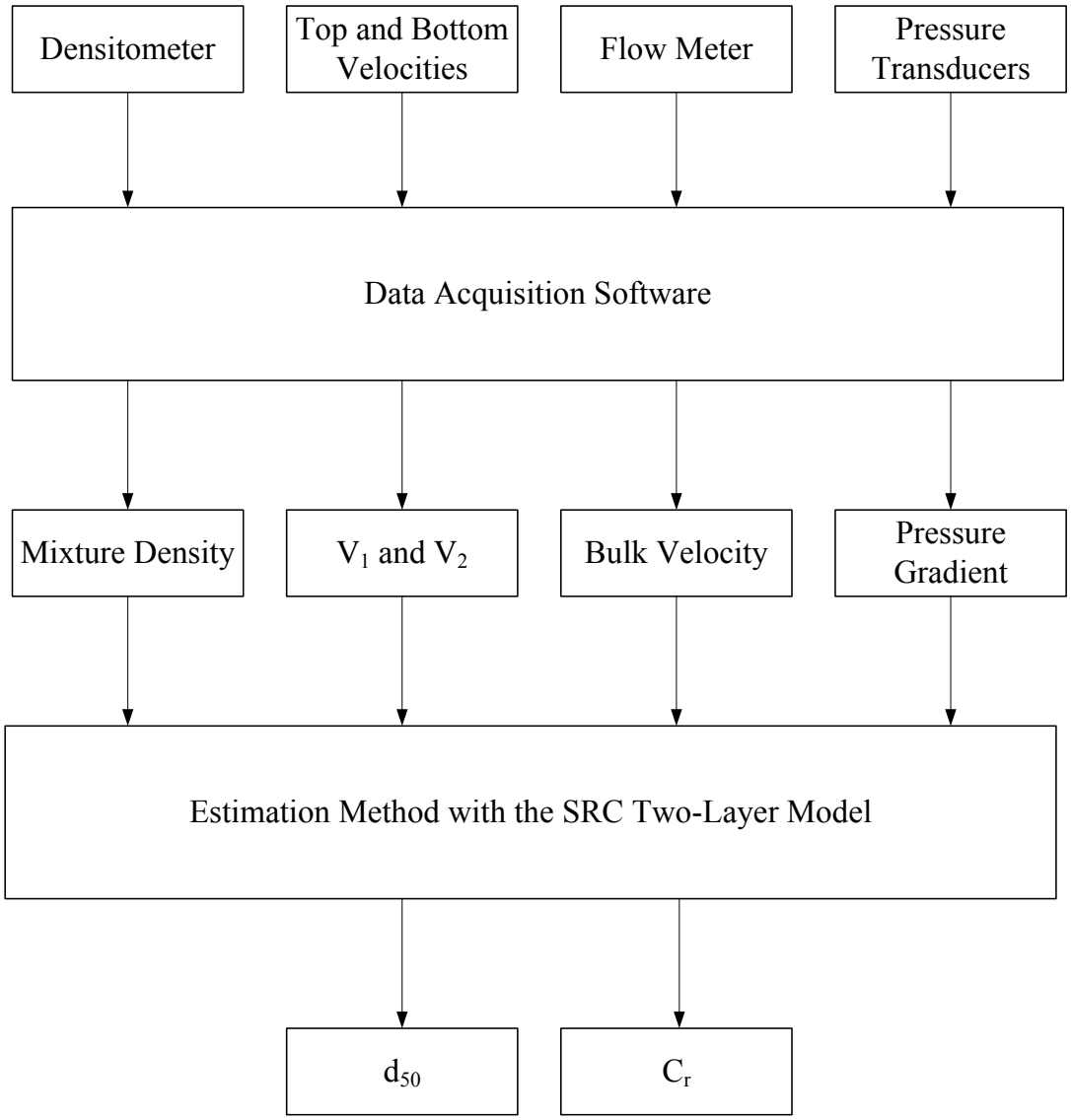

Figure 29: Instrumentation, inputs, and outputs for d_{50} and C_r prediction

There are three flow regions in pipelines; uniformly distributed flow, developing flow, and fully developed flow. They are summarized in Figure 30. In uniformly distributed flow, the slurry is well-mixed, the solids volumetric concentration is considered to be uniform, and the location is after a pump (Gillies, 1991). Between uniformly distributed flow and fully developed flow is developing flow. Developing flow occurs approximately 50 pipe diameters from any flow

disturbances (Gillies, 1991). Recently, it has been debated that developing flow may occur more than 85 pipe diameters from pump outlets (Fuhr et al., 2014).

All instruments in Table 4 should be placed as close to each other as possible, because the estimation method assumes that the inputs are collected from the same pipe axial location and the SRC two-layer model is developed for steady-state flow. This assumption is reasonable as the slurry should not change in fully-developed flow (as long as bulk velocity does not change); however instruments should still be in close proximity and at a location where fully developed flow is established in the event of transient flow conditions. The flow meter is the exception, as volumetric flow rate is constant throughout all sections of the pipeline.

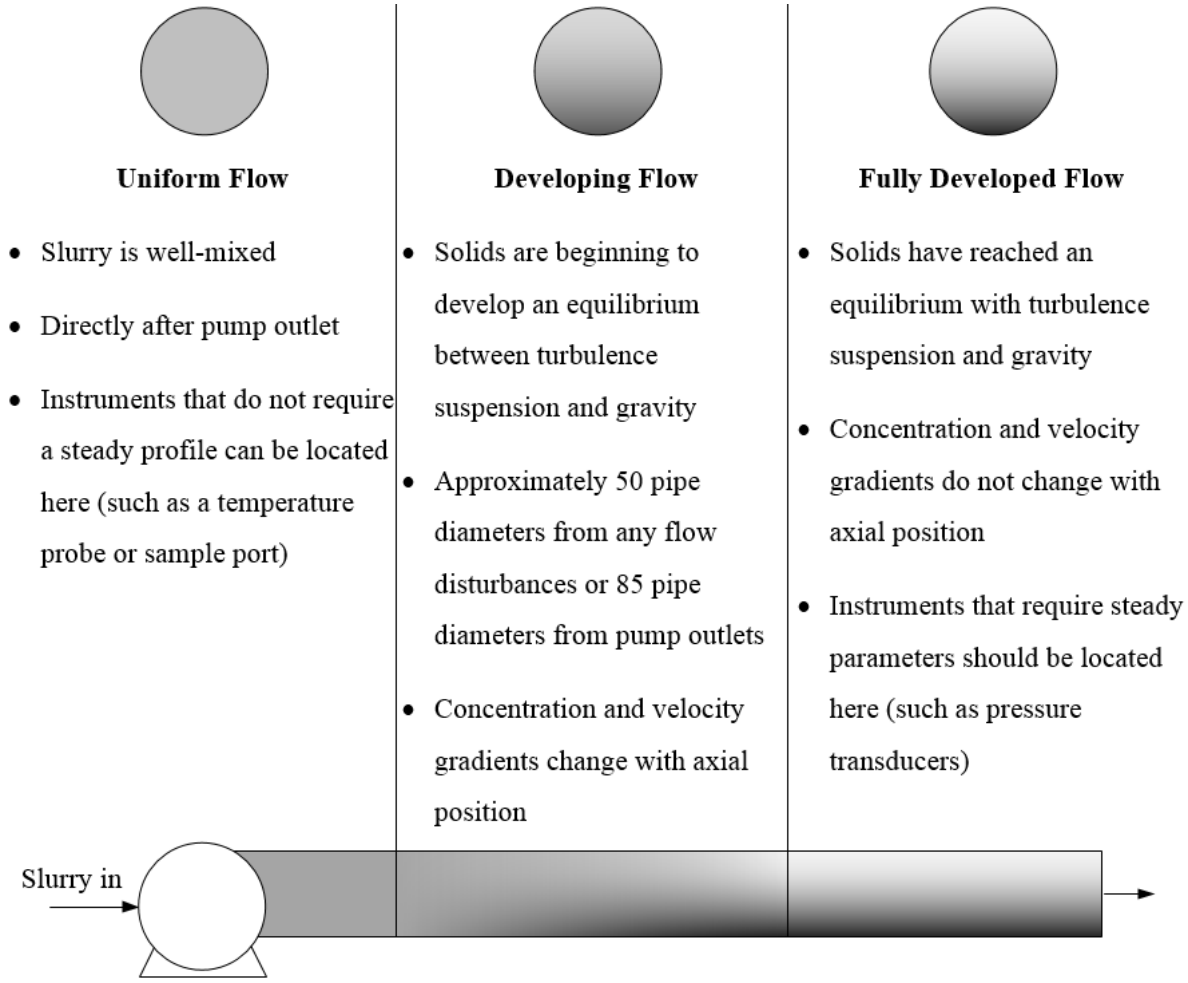

Figure 30: Steady-state flow regions during pipeline operation (Fuhr et al., 2014; Gillies, 1991)

It is possible to have solids properties differ down the length of the pipeline in fully developed flow if different slurry is flowing into the pipeline. Therefore, the maximum "suggested velocity" calculated should be applied for the duration that the slurry is in the pipeline. This ensures that slurry with the highest V_c will leave the pipeline before a lower velocity can be used. The time that a parcel of slurry is transported through a pipeline can be calculated from the residence time, T. The residence time is defined as the average time that one particle will spend in the pipeline.

$$T = \frac{\text{Volume}}{Q} \tag{5.1}$$

where the volume of the pipeline can be calculated by:

$$\text{Volume} = \frac{\pi L D^2}{4} \tag{5.2}$$

Running the estimation method will discretize the pipeline horizontally, as illustrated in Figure 31. This is inaccurate, as slurries will mix, especially the longer the slurry is in the pipeline. This means that the "suggested velocity" calculated with the maximum V_c and held for the duration of the residence time will be conservative. Additionally, this is also why the instruments should be placed as early on in the developed flow region as possible - to ensure that each slurry section is captured before mixing takes place.

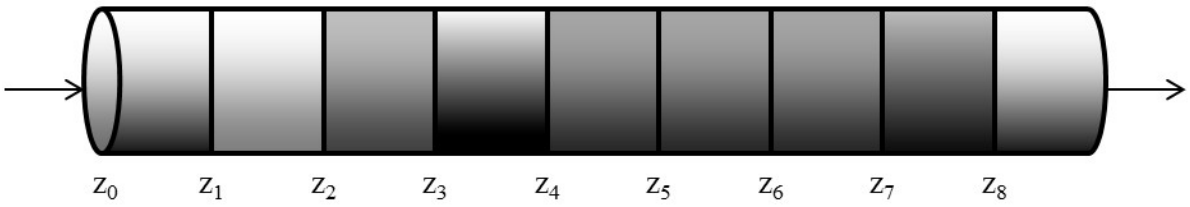

Figure 31: Discretization from using the estimation method

The estimation method requires that V_1 and V_2 be provided as an input. Therefore, an instrument is required to measure top and bottom velocities that can be turned into V_1 and V_2. There are many types of instruments that can be used to measure velocity, such as laser doppler velocimetry (LDV), particle image velocimetry (PIV), electrical probes, Prandtl tubes, acoustic

doppler velocity profilers (ADVP), electrical impedance tomography (EIT), and ultrasonic, acoustic, and sonar velocity sensors (Fredagsvik, 2014; Matousek et al., 2014; Hashemi et al., 2014b; Messa et al., 2014; Hashemi, 2013; Albion et al., 2011; Brücker 2000); however not all instruments are well-suited for this application. Particle image velocimetry cannot measure slurries with solids volume fractions greater than 0.05 (Brücker, 2000). Similarly, LDV cannot measure slurries with higher than 0.15-0.20 solids volumetric concentration (Messa et al., 2014). Electrical probes are process-wetting and measure the solids velocity; however, they are sensitive to flow distortion when placed too close to the pipe wall (Messa et al., 2014). Since the cross-sectional area of the second layer can be quite small relative to the cross-sectional area of the upper layer, the probe would have to be placed close to the pipe invert. Prandtl tubes measure the liquid velocity, and become less accurate at high solids concentrations (Matousek et al., 2014). Acoustic Doppler Velocity Profilers require a suitable "flow depth" (Matousek et al., 2014), which means that the instrument may not be able to be placed close to the pipe invert. Furthermore, EITs are intrusive, whereas ultrasonic, acoustic, and sonar velocity sensors are not process-wetting. Ultrasonic, acoustic, and sonar velocity sensors and EITs are placed around the pipe's circumference, can work for high and low solids concentrations, and do not have flow depth restrictions (Fredagsvik, 2014; Hashemi, 2013; Maron et al., 2008). Ultrasonic, acoustic, and sonar velocity sensors are widely used in the pipeline transportation industry and are already used for solids deposition detection. Therefore, they are the best choice for the d_{50} and C_r estimation method and will be discussed further.

There are many manufacturers of ultrasonic, acoustic, and sonar velocity measurement systems, and further information regarding the technical descriptions and brands can be found in Fredagsvik (2014). CiDRA developed a passive sonar velocity profiler that can measure online

the vertical velocity profile in heterogeneous slurries, and therefore could be used to predict V_1 and V_2 values in this application.

The CiDRA SONARtrac VF-100 reports local velocity signals at circumferential positions corresponding to the top of the pipe, 45°, 90°, 135°, and at the pipe invert (Maron et al., 2008). This corresponds to chord-averaged vertical positions of 1, 0.8, 0.5, 0.2 and 0. The CiDRA meter interpolates between each sensor to produce a velocity profile (Maron et al., 2008). Values from the CiDRA meter can be used to calculate V_1 and V_2. In the SRC two-layer model, V_1 and V_2 are imaginary values that are calculated within the model to predict the pressure gradient. They correspond to an average velocity of the solid and liquid in two imaginary layers, as described earlier.

To determine how the CiDRA meter outputs can correlate to V_1 and V_2, experimental velocity profiles were compared with V_1 and V_2 values calculated from the SRC two-layer model. The experimental velocity profiles were reported by Roco and Shook (1983) and Gillies et al. (2004). Their experimental data can be found in Table 5 and was used in the SRC two-layer model to calculate V_1 and V_2. In both studies, it was reported that the particle size distributions were narrow, and it was assumed that the carrier fluid was water (i.e. $C_f = 0$).

Table 5: Experiments used to find V_1 and V_2 sensor positions

Case	Experiment	D [mm]	ρ_s [kg/m3]	d_{50} [µm]	C_r	V [m/s]
1	Roco and Shook, 1983	51.5	2650	165	0.09	3.78
2	Roco and Shook, 1983	50.7	2650	520	0.12	3.20
3	Roco and Shook, 1983	50.7	2650	520	0.11	4.00
4	Gillies et al., 2004	103.0	2650	90	0.19	1.33
5	Gillies et al., 2004	103.0	2650	90	0.19	2.00
6	Gillies et al., 2004	103.0	2650	90	0.19	3.00

Figure 32 plots the velocity profiles from Roco and Shook (1983) and Gillies et al. (2004) and their corresponding V_1 value calculated from the SRC two-layer model. Table 6 lists the V_1, A_1, V_2, and A_2 values calculated from the SRC two-layer model for the six cases. All V_1 calculations fit within the experimental data. The only V_2 value that fit within the experimental data was for case 6, most likely because the bulk velocity was high enough to have an approximately symmetric vertical velocity profile. The estimation method should check the calculated vertical velocity profile to determine if the profile is symmetric or not when determining V_1 and V_2 values. All other V_2 values did not fit within the data set. This may be due to the size of A_2. Further studies are necessary to determine if the CiDRA sensor at the pipe invert could correlate to V_2. The average V_1 value corresponded to a normalized height location of 0.85 (excluding case 6), and it may be possible to use the velocity profile at this height for V_1.

Additional experiments are required to see if further manipulation of CiDRA values are required to correspond to V_1 and V_2 and if the relations are consistent for all slurry and pipe sizes.

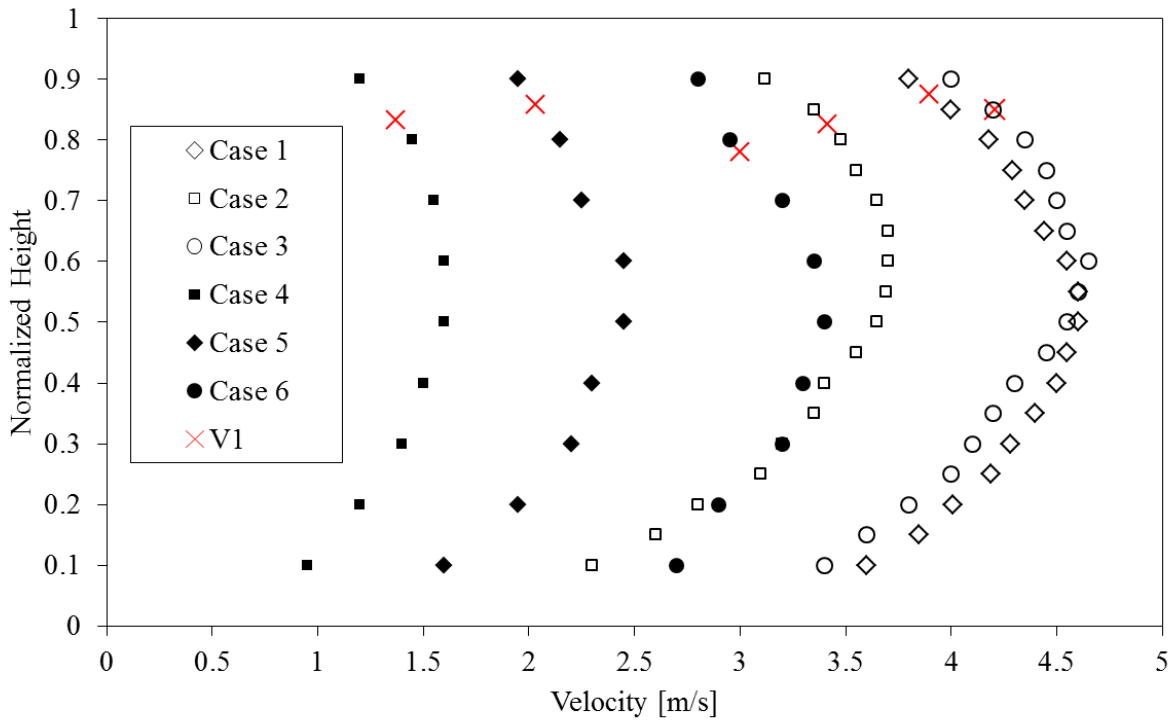

Figure 32: Velocity profiles from Roco and Shook (1983) and Gillies et al. (2004), including the corresponding V_1 and V_2 values calculated from the SRC two-layer model

Table 6: SRC two-layer model values of V_1, A_1/A, V_2, and A_2/A calculated using values from Roco and Shook (1983) and Gillies et al. (2004)

Case	V_1 [m/s]	$\frac{A_1}{A}$	V_2 [m/s]	$\frac{A_2}{A}$
1	3.9	0.91	2.6	0.09
2	3.4	0.79	2.4	0.21
3	4.2	0.81	3.1	0.19
4	1.4	0.95	0.5	0.05
5	2.0	0.97	1.0	0.03
6	3.0	1.00	3.0	0.00

It should also be noted that V_1 and V_2 in the SRC two-layer model represent the average velocity of the mixture in A_1 and A_2, respectively (Matousek, 1997). In reality, the liquid and solids velocities are different (Messa et al., 2014), and the CiDRA meter assumes that they are moving at the same velocity[1]. Therefore, there may be error associated with using the normalized height positions determined from the data from Roco and Shook (1983) and Gillies et al. (2004) as their experiments use an electrical resistivity probe and report a solids velocity profile.

[1] Maron et al. (2008) states that the CiDRA meter measures the flow velocity. In email correspondence with CiDRA technical support on December 4th, 2014, it was communicated that the solids and liquids are assumed to move at the same speed.

5.1. Deposition Detection

It is not recommended to operate at the deposition velocity, because deposition can happen quickly with small changes in solids properties or flow conditions. Therefore, the V_c attained from the predicted d_{50} and C_r should be further manipulated into a "suggested operational velocity." This velocity should be multiplied by a factor of 1.15 for coarse slurries (Hashemi, 2014b) or have an additional 0.3 m/s added for contingency (Thomas, 2014). In reality, it depends partly on the degree of uncertainty in the design/operating parameters (e.g. d_{50}, μ_f, and C_{vd}).

Even when the bulk velocity is greater than the deposition velocity, there is still risk of deposition, due to malfunctioning instrumentation, an unforeseen computational problem, or an incorrect calculation in the residence time. There should be an additional check to ensure that deposition does not occur. There are many ways that solids deposition can be detected. The most applicable to this study is the CiDRA meter.

The CiDRA meter measures local velocity at each sensor and develops a vertical velocity profile with interpolation, as illustrated in Figure 33. The x axis is the normalized velocity, which was calculated by normalizing the velocities to the centerline velocity. This was done to easily compare the changes in vertical velocity profile shape as the flow becomes more stratified (Maron et al., 2008). The figure was generated with 186 μm slurry. In homogeneous flow, the center of the pipe corresponds to the largest velocity, and the vertical velocity profile is approximately symmetric. If the pipeline is operating in homogeneous flow, the CiDRA sensors at the bottom and top of the pipe will report approximately the same velocity (corresponding to

the solid line in Figure 33). In heterogeneous flow, the vertical velocity profile becomes asymmetric and the flow is more stratified than in homogeneous flow (dotted-dashed line). Before deposition occurs, but while still in heterogeneous flow, highly stratified velocity profiles are measured (dotted line). The top sensors report velocities higher than the center velocities. The sensor at the invert cannot detect movement when solids settle, and reports velocities that are similar or higher than the sensor at 135° (the next lowest sensor) (Maron et al., 2008). This is called an inverted velocity profile (Maron et al., 2008), as seen on the dashed line in Figure 33. The flow at the top sensor is now even faster than the center velocity. Therefore, it is possible to detect deposition when this instrument reports an inverted velocity profile.

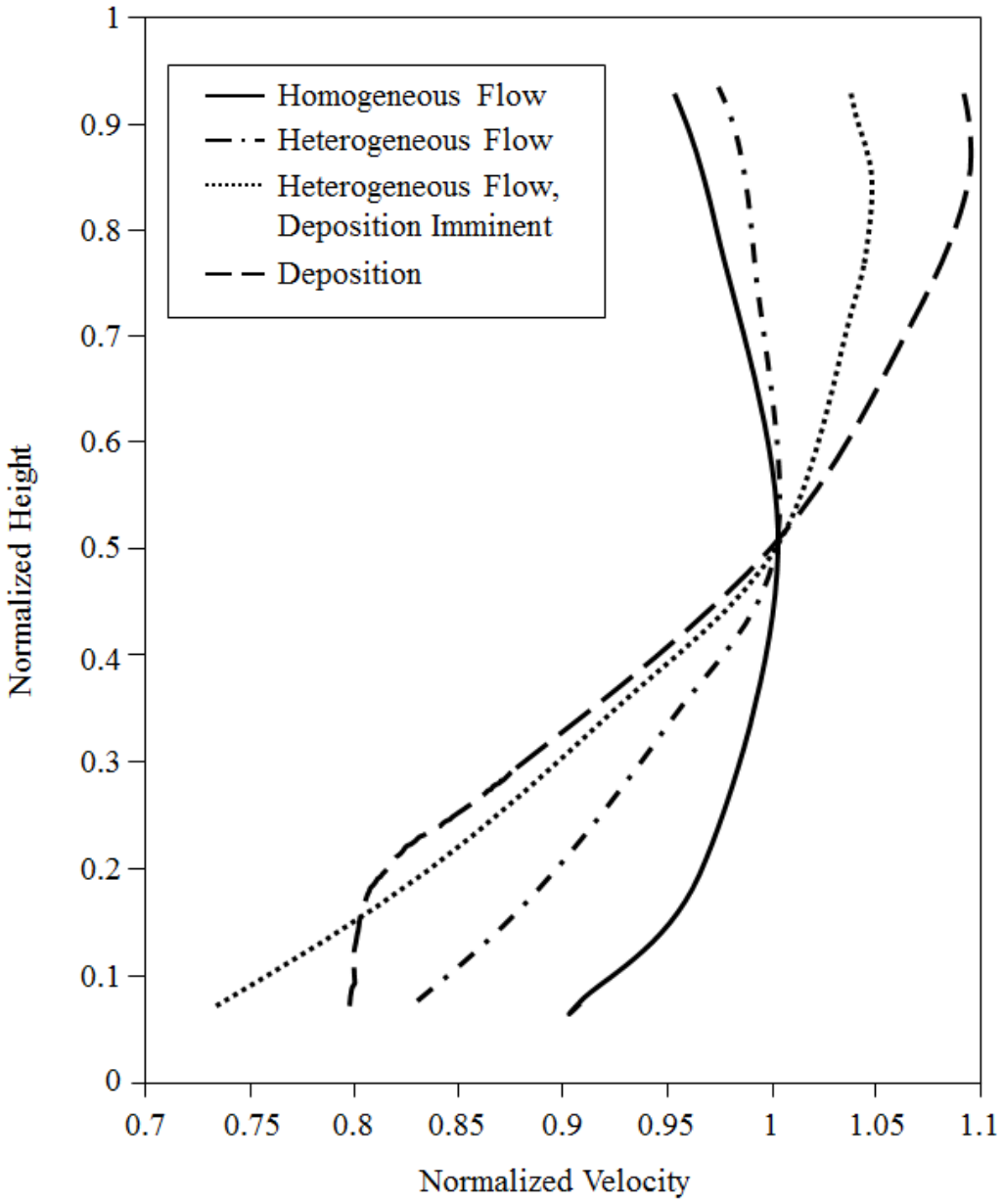

Figure 33: Shapes of CiDRA meter velocity profiles to detect deposition (Maron et al., 2008)

6 Summary and Conclusions

An estimation method was developed to predict the coarse solids median particle size and concentration using the slurry pipeline parameters of flowrate, pressure gradient, local velocities, and total solids concentration. The predicted coarse solids median particle size and concentration were used as inputs to predict the deposition velocity and specific energy consumption (SEC).

The estimation method consisted of using equations from the Saskatchewan Research Council (SRC) two-layer model in an interior-point optimization algorithm. An interior-point algorithm was used, because the problem was poorly-scaled and too complicated for analytical Hessian calculations. Every time the estimation method was performed, the pressure gradient, velocities of Layer 1 and Layer 2, flow rate, and mixture density must be updated. These parameters are held constant during optimization, and updated at the frequency that the estimation method is required to run. The decision variables are the coarse solids median particle size and concentration. The objective function was the square of the calculated Layer 1 pressure gradient subtracted from the provided pressure gradient. An equality constraint was also used to ensure that the pressure gradient of Layer 1 and Layer 2 were equal. Constraints were also placed on the coarse solids median particle size and concentration to ensure that the particles were not outside the range of typical slurry found in the mining and oil sands industry, that a particle size distribution (PSD) was not predicted with too many fines, and that the predicted coarse solids concentration was not higher than the total solids concentration.

The estimation method was simulated with ideal values calculated from the SRC two-layer model. The prediction results were compared with the values that were placed into the SRC two-layer model. The estimation method predicted the trends well. The coarse solids median particle size and concentration were predicted with an average 13.6% and 4.2% accuracy, respectively. Errors are caused by regions of low curvature along the coarse solids median particle size axis, and Coulombic friction having many local optimums.

It is possible to use this estimation method on a real pipeline with instrumentation. A pressure transducer is required for the pressure gradient, a velocity profiler for Layer 1 and Layer 2 velocities, a flowmeter for the bulk flow rate, and a densitometer for the mixture density. Information about the pipeline and slurry that is not expected to change much, such as the pipeline diameter, solids maximum packing, and liquid carrier properties can be updated manually.

Once a coarse solids medium particle size and concentration is known, the deposition velocity and minimum SEC can be calculated. This can be used to determine a suggested operational velocity that the pipeline can operate at. The suggested operational velocity corresponds to a velocity slightly higher than the minimum SEC, which will reduce energy usage without causing deposition. Error propagated through the deposition velocity and SEC calculations. There was an average error of 5.5% for V_c predictions. The predicted V_c multiplied by a safety factor of 1.15 gave a suggested operational velocity for the pipeline. The predicted SEC matched known SEC trends well and the predicted and known minimum SEC corresponded graphically.

The estimation method is limited to assumptions placed on the SRC two-layer model. These assumptions include turbulent pipe flow, a horizontal pipeline, and the coarse solids median particle size representing the size of all of the coarse particles in the slurry (Saskatchewan Research Council, 2014). Consequently, this method works best for narrow PSDs. Additionally, the estimation method can only predict slurry properties under steady-state conditions. All instrumentation must be placed in fully-developed flow. The estimation method does not consider turbulent mixing as the slurry moves down the pipeline.

6.1 Future Work

For future work, the interior-point optimization algorithm should be iterated with different starting points. Additionally, future research is required to determine methods to propagate uncertainty in order to provide uncertainty bounds for the predictions.

The simulation can be validated by doing experiments on a pipeline. A CiDRA meter can be used to predict Layer 1 and Layer 2 velocities; however experiments should take place to determine the best measurement location and method for determining how the CiDRA meter measurements relate to Layer 1 and Layer 2 velocities. Alternatively, a system of first order elliptical PDEs can be used to predict the velocity profile instead of instrumentation. The additional properties calculated from the PDE system could be used as constants in the estimation method rather than being calculated during optimization.

A different constrained nonlinear multivariate optimization problem could also be constructed with d_{50}, C_r, V_1, and V_2 as the decision variables. The error could be compared to when V_1 and V_2 is provided.

An online PSD prediction is a natural extension of this estimation method. An SRC multispecies model set for release in 2015 includes a PSD input, which can be used as decision variables in this estimation method. The equations in the SRC two-layer model that rely on d_{50} could also be discretized to represent different sections of a PSD. A multivariable optimization model can be written such that each discretized section becomes a decision variable. An appropriate averaging technique could then be used on the set of results to yield a PSD.

References

Adhya, N., M. Tawarmalani, and N.V. Sahinidis, "A Lagrangian Approach To The Pooling Problem", Industrial & Engineering Chemistry Research 38.5 (1999): 1956-1972.

Albion, K., L. Briens, C. Briens, and F. Berruti, "Multiphase Flow Measurement Techniques For Slurry Transport", International Journal Of Chemical Reactor Engineering 9 (2011): 5.

Bergman, T. L., D.P. Dewitt, F.P. Incropera, and A.S. Lavine. Fundamentals Of Heat And Mass Transfer. 7th ed. Jefferson City, United States: Wiley, 2011. 231-235, 389.

Bertsekas, D.P.. Nonlinear Programming. 2nd ed. Belmont, Mass.: Athena Scientific, 1999. 63, 64, 234, 370, 371, 373.

Brown, N.P., "Flow Regimes of Settling Slurries in Pipes" Slurry Handling: Design of Solid-liquid Systems, Essex, England: Elsevier Science Publishing Co, 1991. 44.

Brücker, C. "PIV In Two-Phase Flows", Lecture Series 2000-01, Particle Image Velocimetry and Associated Techniques. Ed. M.L. Riethmuller. 17-21 January 2000, Von Karman Institute For Fluid Dynamics. Rhode-St. Genese, Belgium (2000): 1051-1054.

Buckwalter, R.R., "Control of Slurry Pipeline Systems" Slurry Handling: Design of Solid-liquid Systems, Essex, England: Elsevier Science Publishing Co, 1991. 491.

Budak, B.M., A.A. Samarskii, and A.N. Tikhonov. A Collection Of Problems On Mathematical Physics. Trans. A.R.M. Robson. Poland: Pergamon Press, 1964.

Byrd, R.H., J.C. Gilbert, and J. Nocedal, "A Trust Region Method Based On Interior Point Techniques For Nonlinear Programming", Mathematical Programming 89.1 (2000): 149-185.

Crowe, C. R. E. Multiphase Flow Handbook, Boca Raton, Florida: Taylor & Francis, 2006. 1-10, 1-12, 4-52, 4-68.

De Nevers, N, Fluid Mechanics For Chemical Engineers, 3rd Ed. Boston: McGraw-Hill Higher Education, 2005. 89, 175, 177.

Derammelaere, R., E.J. Wasp, N. Neal, and W.M. Cauthen, “The history of coal slurry pipelines", 19th International Conference on Hydrotransport. Ed. R.S. Sanders and R. Sumner. Proceedings from Hydrotransport 19, 24-26 September 2014, Colorado School of Mines. Golden, Colorado: The BHR Group (2014): 264.

Dighade, R.R., Estimation of deposition velocity in the flow of multisized particulate slurries through pipes. Visvesvaraya National Institute of Technology, Nagpur: M.Tech Project Thesis, Dept. of Hydraulic Engineering (1999).

DuChateau, P., and D.W. Zachmann. Applied Partial Differential Equations. New York: Harper & Row, 1989. 31, 327-335.

Dullerud, G.E., and F.G. Paganini, A Course In Robust Control Theory : A Convex Approach, New York: Springer, 2000. 32, 33.

Durand, R. and E. Condolios, “Experimental Study of the Hydraulic Transport of Coal and Solid Materials in Pipes”, Proc. Colloq. On the Hydraulic Transport of Coal, U.K.: Nat. Coal Board, Paper IV (1952): 39-55.

Edgar, T.F., D.M. Himmelblau, and L.S. Lasdon, Optimization Of Chemical Processes, New York: McGraw-Hill, 2001. 4, 124, 128, 137, 138, 189, 191, 192, 194, 207, 286, 291, 292, 306, 324.

El-Farra, N.H., A. Armaou, and P.D. Christofides, "Analysis And Control Of Parabolic PDE Systems With Input Constraints", Automatica 39.4 (2003): 715-725.

Fredagsvik, K., Use of ultrasonic and acoustic sensors for characterization of liquid-particle flow and evaluation of hole cleaning efficiency. University of Stavanger: M.Sc. Thesis, Dept. of Petroleum Engineering (2014): 38, 43, 59, 62, 71.

Fritz, J. Partial Differential Equations. 4th ed. New York: Springer-Verlag, 1982. 34, 37, 46, 47

Forbes, F.J., and I. Aksikas, “Chapter II: Linear Programming”, Engineering Optimization. University of Alberta, Edmonton, AB. Spring, 2010a. Lecture.

Forbes, F.J., and I. Aksikas, “Chapter IV: Unconstrained Multivariate Optimization”, Engineering Optimization. University of Alberta, Edmonton, AB. Spring, 2010b. Lecture.

Fuhr, A., M. Krantz, and B. Fotty, "An investigation into developing slurry flow conditions and their effect on wear profiles using a pilot scale flow loop", 19th International Conference on Hydrotransport. Ed. R.S. Sanders and R. Sumner. Proceedings from Hydrotransport 19, 24-26 September 2014, Colorado School of Mines. Golden, Colorado: The BHR Group (2014): 325.

Gillies, D.P., Particle Contributions To Kinematic Friction In Slurry Pipeline Flow. University of Alberta: M.Sc. Thesis, Dept. of Chemical Engineering (2013): 15, 57.

Gillies, R.G. "Flow Loop Studies." Slurry Handling: Design Of Solid-Liquid Systems. Ed. Nigel P. Brown and Nigel I. Heywood. New York: Elsevier Applied Science, 1991. 195, 199, 200.

Gillies, R.G., Pipeline Flow of Coarse Particle Slurries. University of Saskatchewan: Ph.D. Thesis, Dept. of Chemical Engineering (1993): 1, 54.

Gillies, R. G., W. H. W. Husband and M. H. Small, A Study of Flow Conditions Arising in Horizontal Coarse Slurry Pipeline Practice. Phase I, Report R-832-2-C-85. Saskatoon, Saskatchewan: Saskatchewan Research Council, 1985.

Gillies, R.G., J. Schaan, R.J. Sumner, M.J. McKibben, and C.A. Shook, "Deposition velocities for Newtonian slurries in turbulent flow", The Canadian Journal Of Chemical Engineering 78, no. 4 (2000): 704-708.

Gillies, R.G., and C.A. Shook. "Concentration Distributions Of Sand Slurries In Horizontal Pipe-Flow." Particulate Science And Technology 12.1 (1994): 45-69.

Gillies, R.G. and C.A. Shook, "Modelling high concentration settling slurry flows", The Canadian Journal Of Chemical Engineering 78 (2000): 709–716.

Gillies, R.G., C.A. Shook and K.C. Wilson, "An Improved Two Layer Model For Horizontal Slurry Pipeline Flow", The Canadian Journal Of Chemical Engineering 69.1 (1991): 173-178.

Gillies, R.G., C.A. Shook and J. Xu, "Modelling heterogeneous slurry flows at high velocities", The Canadian Journal Of Chemical Engineering 82 (2004): 1060-1065.

Gillies, R.C., M. McKibben, K. Hill and C.A. Shook, "Sand Transport by Newtonian Fluids in Laminar Pipe Flow", Powder Technology 104 (1999): 269-277.

Goosen, P., Ilgner, H., and Dumbu, S. "Settlement in backfill pipelines: its causes and a novel online detection method", Minefill 2011, 10th International Symposium on Mining with Backfill, The Southern African Institute of Mining and Metallurgy, 2011

Griva, I., S.G. Nash, and A. Sofer, Linear And Nonlinear Optimization, Philadelphia: Society for Industrial and Applied Mathematics, 2012. 5.

Grzina, A., A. Roudnev, and K.E. Burgess. Slurry Pumping Manual. 1st Ed. Warman International LTD., 2002.

Harris, J. and R. Talamudupula, "The effects of solids porosity on physical properties and slurry behaviour", 19th International Conference on Hydrotransport. Ed. R.S. Sanders and R. Sumner. Proceedings from Hydrotransport 19, 24-26 September 2014, Colorado School of Mines. Golden, Colorado: The BHR Group (2014): 493.

Hashemi, S.A., Velocity And Concentration Fluctuations In Concentrated Solid-Liquid Flows. University of Alberta: Ph.D. Thesis, Dept. of Chemical Engineering (2013): 3, 6-8, 28, 29, 31, 35, 39, 49, 93, 128, 129.

Hashemi, S.A., R.B. Spelay, K.F.K. Adane, and R.S. Sanders, "Solids velocity fluctuations in concentrated slurries", 19th International Conference on Hydrotransport. Ed. R.S. Sanders and R. Sumner. Proceedings from Hydrotransport 19, 24-26 September 2014, Colorado School of Mines. Golden, Colorado: The BHR Group (2014a): 391-403.

Hashemi, S.A., R.S. Sanders, K.C. Wilson, "Specific Energy Consumption And Optimum Operating Condition For Fine-Particle Slurries", 18th International Conference on Hydrotransport. Proceedings from Hydrotransport 18, 22-24 September 2010, The Intercontinental Hotel. Rio de Janeiro, Brazil: The BHR Group (2010).

Hashemi, S.A., K.C. Wilson, and R.S. Sanders, "Specific Energy Consumption And Optimum Operating Condition For Coarse-Particle Slurries", Powder Technology 262 (2014b): 183-187.

Hedengren, J., “Interior Point Methods”, ME 575 – Optimization Methods. Brigham Young University, Provo, Utah. April 07, 2014. Lecture.

Hoffman, J. D. Numerical Methods For Engineers And Scientists, New York: Marcel Dekker, 2001. 504, 505, 507, 509-511.

Huggett, A.G. "Transient Pipe Flow Behaviour." Slurry Handling: Design Of Solid-Liquid Systems. Ed. Nigel P. Brown and Nigel I. Heywood. New York: Elsevier Applied Science, 1991. 183.

Ilgner, H.J., “On-line Measurements of Critical Deposition Velocities for Flow Optimisation", Rise of the Machines: The State of the Art in Mining, Mechanisation, Automation, Hydraulic Transportation and Communications Conference. 14-16 March 2006: The South African Institute of Mining and Metallurgy (2006): 1-24.

Ilgner, H.J., “Novel instrumentation to detect sliding and erratic bed load motion", 19th International Conference on Hydrotransport. Ed. R.S. Sanders and R. Sumner. Proceedings from Hydrotransport 19, 24-26 September 2014, Colorado School of Mines. Golden, Colorado: The BHR Group (2014): 163-178.

Jeffrey, A. Applied Partial Differential Equations: An Introduction. Academic Press, 2002. 60, 219-223.

Kalekudithi, E., R.S. Sanders, K. Nandakumar, and J.H. Masliyah. "Hydrodynamic Simulation Of Horizontal Slurry Pipeline Flow Using ANSYS-CFX." Industrial & Engineering Chemistry Research 48.17 (2009): 8159-8171.

Kaushal, D. R., and Y. Tomita. "Prediction Of Concentration Distribution In Pipeline Flow Of Highly Concentrated Slurry." Particulate Science & Technology 31.1 (2013): 28-34.

King, R. P. Introduction To Practical Fluid Flow. Boston: Butterworth-Heinemann, 2002. 83.

Krampa, F.N., Two-Fluid Modelling of Heterogeneous Coarse Particle Slurry Flows. University of Saskatchewan: Ph.D. Thesis, Dept. of Mechanical Engineering (2009): 6-9.

Maron, R.J., Fernald, M., O'Keefe, C., Viega, J. and Bailey, T. "New Applications of Sonar-Based Technology in The Minerals Processing Industry: Velocity Profile Measurement and Pipe Wall Wear Monitoring in Hydrotransport Lines" CiDRA Minearls Processing Corp., Wallingford, CT (2008)

Matousek, V., "On A Solid Particle Suspension In A Slurry Pipeline", Advances In Fluid Mech. Int. Conf. New Orleans: WIT Press, 1996. 317-326.

Matousek, V., Flow Mechanism of Sand-Water Mixtures, Delft University, The Netherlands: Ph.D. Thesis (1997): 5, 17, 40, 43, 44, 46, 47, 102, 104, 126, 252.

Matousek, V., "Chapter 3. Flow of soil-water mixture", Dredge Pumps and Slurry Transport. Delft University of Technology, Open Course Ware. October 13, 2004. Lecture.

Matousek, V., V. Bareš, J. Krupička, T. Picek, and Š. Zrostlík, "Experimental evaluation of interfacial friction and transport in steep flume", 19th International Conference on Hydrotransport. Ed. R.S. Sanders and R. Sumner. Proceedings from Hydrotransport 19, 24-26 September 2014, Colorado School of Mines. Golden, Colorado: The BHR Group (2014): 377-390.

Messa, G.V., and S. Malavasi. "Numerical Investigation Of Solid-Liquid Slurry Flow Through An Upward-Facing Step." Journal Of Hydrology And Hydromechanics 61.2 (2013): 126-133.

Messa, G.V., M. Malin, and S. Malavasi. "Numerical Prediction Of Fully-Suspended Slurry Flow In Horizontal Pipes." Powder Technology 256 (2014): 61-70.

Moghadam, A.A. Infinite-Dimensional LQ Control For Combined Lumped And Distributed Parameter Systems, University of Alberta: Ph.D. Thesis, Dept. of Chemical Engineering (2013): 1, 3.

Munusamy, S., S. Narasimhan, and N. S. Kaisare. "Order Reduction And Control Of Hyperbolic, Countercurrent Distributed Parameter Systems Using Method Of Characteristics." Chemical Engineering Science 110 (2014): 153-163.

Newitt, D.M., J.F. Richardson, M. Abbott, and R.B. Turtle, "Hydraulic Conveying of Solids in Horizontal Pipes", Trans. Inst. Chem. Eng. 33 (1955): 93-113.

Nocedal, J., and S.J. Wright, Numerical Optimization, New York: Springer, 2006. 2-7, 26, 27, 393, 565, 570, 572.

Paterson and Cooke. The Design of Slurry Pipeline Systems. 8th Revision. Pinelands, South Africa: Paterson & Cooke, 2014. 2.14-16, 3.8, 6.15.

Ray, W. H. Advanced Process Control. New York: McGraw-Hill, 1980. 140.

Rhee, H.K., R. Aris and N. R. Amundson. First-order Partial Differential Equations. Vol. I. Englewood Cliffs, NJ: Prentice-Hall, 1986.

Rhodes, M. J. Introduction To Particle Technology. Chichester, England: Wiley, 2008. 2.

Rice, H., "Transport and deposition behaviour of model slurries in closed pipe flow." University of Leeds, England: Ph.D. Thesis (2013): 31, 32.

Roco, M.C., and C.A. Shook, "Modeling Of Slurry Flow: The Effect Of Particle Size", The Canadian Journal Of Chemical Engineering 61.4 (1983): 494-503.

Sanders, R.S., “3.6.2 Friction loss calculations – Lecture #27 and Seminar #6”, Introduction to Fluid-Particle Systems. University of Alberta, Edmonton, AB. 19-20 March, 2012. Lecture.

Sanders, R.S., J. Schaan, R. Hughes, and C.A. Shook, "Performance Of Sand Slurry Pipelines In The Oil Sands Industry", The Canadian Journal Of Chemical Engineering 82.4 (2004): 850-857.

Saskatchewan Research Council, Slurry Pipeline Systems Course, 13-16 May, 2014. Saskatoon, SK, Canada: SRC Pipe Flow Technology Centre, 2014. 7, 17, 18, 20, 24, 25.

Schaan, J., N. Cook, and R.S. Sanders, “On-line wear measurements for commercial-scale, coarse-particle slurry pipelines", 17th International Conference on Hydrotransport. Proceedings from Hydrotransport 17, 7-11 May 2007, Boe Centre. Cape Town, South Africa: The Southern African Institute of Mining and Metallurgy and the BHR Group (2007). 291-300.

Seborg, D., T. Edgar, D. Mellichamp, and F. Doyle III. Process Dynamics And Control. 3rd ed. Hoboken, N.J.: John Wiley & Sons, 2011. 318.

Shang, H. Characteristic-Based Control Of Distributed Parameter Systems. University of Alberta: Ph.D. Thesis, Dept. of Chemical Engineering (2002): 19-22, 112-116.

Shang, H., F.J. Forbes, and M. Guay, "Computationally Efficient Model Predictive Control For Convection Dominated Parabolic Systems", Journal Of Process Control 4 (2007): 379.

Sinkov, K.F., P.E. Spesivtsev, and A.A. Osiptsov, "Simulation of particles transport in multiphase pipe flow for cleanup of oil and gas wells", 19th International Conference on Hydrotransport. Ed. R.S. Sanders and R. Sumner. Proceedings from Hydrotransport 19, 24-26 September 2014, Colorado School of Mines. Golden, Colorado: The BHR Group (2014): 5-16.

Smith, J., Measurement of Carrier Fluid Viscosities for Oil Sand Extraction and Tailings Slurries. University of Alberta: M.Sc. Thesis, Dept. of Chemical Engineering (2013): 21.

Spelay, R., R.G. Gillies, S.A. Hashemi, and R.S. Sanders, “Effect of pipe inclination on the deposition velocity of settling slurries", 19th International Conference on Hydrotransport. Ed. R.S. Sanders and R. Sumner. Proceedings from Hydrotransport 19, 24-26 September 2014, Colorado School of Mines. Golden, Colorado: The BHR Group (2014): 149.

Spelay, R., S. Hashemi, R.G. Gillies, R. Hegde, R.S. Sanders, and D. Gillies, "Governing Friction Loss Mechanisms and The Importance Of Off-Line Characterization Tests In The Pipeline Transport Of Dense Coarse-Particle Slurries", Proceedings Of The ASME Fluids Engineering Division Summer Meeting, Incline Village, Nevada: ASME (2013).

Shook, C.A., R.G. Gillies, and R.S. Sanders, Pipeline Hydrotransport with Applications In The Oil Sand Industry, Saskatoon, Saskatchewan: SRC Pipe Flow Technology Centre, 2002. 4-1, 4-3, 6-1 - 6-5.

Shook, C.A., R.G. Gillies, M. Small, and W.H.W. Husband, Sliding coefficient of friction experimental measurements. Saskatoon, Saskatchewan: SRC Publication E-725-9-C-82, (1982).

Shook, C. A. and M.A. Roco, Slurry Flows: Principles and Practice, Boston: Buttherworth-Heinemann, 1991. 96, 120.

Speranza, A. "Suspension Flows in a Pipeline with Partial Phase Separation." Mathematical And Computer Modelling 33.4-5 (2001): 445-467.

The MathWorks, Inc., R2014a Documentation Center: fmincon, The MathWorks, Inc., 2014. Web. 8 Oct. 2014a. http://www.mathworks.com/help/optim/ug/fmincon.html

The MathWorks, Inc., R2014a Documentation Center: Tolerances and Stopping Criteria, The MathWorks, Inc., 2014. Web. 8 Oct. 2014b. http://www.mathworks.com/help/optim/ug/tolerances-and-stopping-criteria.html

Thomas, A.D., "Slurries of most interest to the mining industry flow homogeneously and the deposit velocity is the key parameter", 19th International Conference on Hydrotransport.

Ed. R.S. Sanders and R. Sumner. Proceedings from Hydrotransport 19, 24-26 September 2014, Colorado School of Mines. Golden, Colorado: The BHR Group (2014): 251.

Vlasak, P., Z. Chara, J. Konfrst, and J. Krupicka, "Effect of concentration and velocity on conveying of coarse grained mixtures in pipe", 24th International Ocean and Polar Engineering Conference, 15-20 June 2014. Busan, Korea: The International Society of Offshore and Polar Engineers (2014): 66.

Wilson, K. C., "Stationary Deposits and Sliding Beds in Pipes Transporting Solids", Proc. 1st Int. Conf. on the Hydraulic Transport of Solids in Pipes, Cranfield. U.K.: BHRA Fluid Engineering, Paper C3 (1970a): 28-40.

Wilson, K.C., "Slip point of beds in solid-liquid pipeline flow", Journal of the Hydraulic Division, ASCE 96(HY1), (1970b): 1-12.

Wilson, K.C., "A Unified Physically Based Analysis of Solid-Liquid Pipeline Flow", in "Proc. 4th Int. Conf. on Hydraulic Transport of Solids", Proc. 4th Int. Conf. on the Hydraulic Transport of Solids in Pipes, Cranfield, U.K.: BHRA Fluid Engineering, Paper A1 (1976): 1-16.

Wilson, K. C., G.R. Addie, and R. Clift, Slurry Transport Using Centrifugal Pumps, 35th Ed. New York: Springer, (2005): 36, 37, 90, 95, 96, 98, 99, 103, 373.

Wilson, K.C., M. Streat, and R.A. Bantin, "Slip-model correlation of dense two-phase flow", Proceedings from Hydrotransport 2, Cranfield, UK: BHRA Fluid Engineering (1972): B1-1-10.

Nomenclature

A	Cross-sectional pipe area [m^2]
A_1	Cross-sectional area of Layer 1 (turbulence forces only) [m^2]
A_2	Cross-sectional area of Layer 2 (turbulence and Coulombic forces) [m^2]
Ar	Archimedes number
c	Local volumetric solids concentration
C	Volumetric concentration of solids, input
C_1	Volumetric concentration of Layer 1 or of solids corresponding to suspension load
C_2	Volumetric concentration of Layer 2, C_1+C_{2c}
C_{2c}	Volumetric concentration of solids in contact load of Layer 2
C_c	Volumetric concentration of solids in contact load
C_D	Drag Coefficient
C_f	Volumetric concentration of fine particles in the liquid as though there is no coarse solids
C_{max}	Volumetric concentration of solids in a settled bed
C_r	Volumetric concentration of coarse particles, particle size greater than 74 μm
C_{rf}	Volumetric concentration of fine particles, particle size less than 74 μm
C_t	Total volumetric solids concentration
C_{vd}	Delivered solids concentration

D	Pipeline inner diameter [m]
d_{12}	Particle diameter at Layer 1 and Layer 2 interface [m]
d_{50}	Median particle diameter of coarse particles [m]
d^+	Dimensionless particle diameter
F	Froude number
F_2	Coulombic friction [Pa]
f_{12}	Interfacial friction factor
f_f	Fluid friction factor
f_s	Particle friction factor
g	Gravity, 9.81 [m^2/s]
k	Hydraulic roughness [m]
$k1$	Parameter for interfacial friction factor
M_{12}	Momentum transfer from Layer 1 to Layer 2 [kg m/s]
M_{21}	Momentum transfer from Layer 2 to Layer 1 [kg m/s]
m_{s12}	Mass transfer of solids from Layer 1 to Layer 2 [kg/s]
m_{s21}	Mass transfer of solids from Layer 2 to Layer 1 [kg/s]
P	Pressure [Pa]
P_{sensor}	Measured pressure gradient [Pa/m]
Q	Flow rate [m^3/s]

r	Interior-point barrier parameter
S_1	Partial parameter of top of Layer 1 [m]
S_2	Partial parameter of bottom of Layer 2 [m]
S_{12}	Length of Layer 1 and Layer 2 interface [m]
t	Time, independent variable [s]
V	Bulk velocity [m/s]
V_1	Average velocity of Layer 1 [m/s]
V_2	Average velocity of Layer 2 [m/s]
V_c	Deposition velocity [m/s]
v_s	Local time averaged vertical particle velocity [m/s]
V_∞	Terminal settling velocity [m/s]
x	Control states
y	Vertical distance [m]
Z	Objective function
z	Horizontal distance [m]

Greek Symbols

α	Angle normal to pipe wall [radians]
β	Angle defining interface of Layer 1 and 2 [radians]
ε_s	Particle diffusivity [m^2/s]
η_s	Coefficient of friction between particles and the pipe wall [dimensionless]
λ	Linear solids concentration [dimensionless]
μ_f	Viscosity of the fluid (liquid and fines) [Pa.s]
μ_L	Viscosity of the liquid (no solids) [Pa.s]
μ_m	Viscosity of the mixture [Pa.s]
ρ_1	Density of Layer 1 [kg/m^3]
ρ_f	Density of fluid (liquid and fines) [kg/m^3]
ρ_L	Density of liquid (no solids) [kg/m^3]
ρ_m	Density of the mixture [kg/m^3]
ρ_s	Density of the solids [kg/m^3]
σ	Normal stress at the pipe wall [Pa]
T	Residence time [s]
τ_1	Kinematic stress of Layer 1 [Pa]
τ_2	Kinematic stress of Layer 2 [Pa]
τ_{12}	Interfacial stress [Pa]

τ_c Shear stress from particle-wall contact [Pa]